Interaction Notes

Note 142

August 1973

# FIELD PENETRATION INTO A SPHERICAL CAVITY

T. B. A. Senior and G. A. Desjardins
The University of Michigan Radiation Laboratory
Department of Electrical and Computer Engineering
Ann Arbor, Michigan 48105

## Abstract

A thin, perfectly conducting, spherical shell having a circular aperture is illuminated by a plane (c.w.) electromagnetic wave at symmetrical incidence. Using a formulation of the problem which is, in principle, exact, a computer program previously developed for the determination of the scattered fields is modified to permit the calculation of the fields within the cavity. Data are presented for a variety of cases and compared with the results of approximate methods.

## 1. Introduction

A problem of considerable interest in EMP studies is the penetration of an electromagnetic field through an aperture in a finite cavity. Unfortunately, it is also a problem of great difficulty with which little progress has been made even in the most elementary situations. One of the main reasons for this is the coupling between the aperture and the cavity, and given the difficulty of treating the problem of an aperture in an infinite screen, it is not surprising that the determination of the fields which couple into a cavity has so far defied rigorous solution.

There is, however, a simple case which can be formulated precisely and then solved numerically to yield data which are, in principle, exact. The geometry is admittedly an idealised one but the problem does have interest in its own right. More importantly, however, the solution can be used to test the accuracy of approximate methods which could be applicable in other, more practical, situations.

The problem considered here is that of a thin, perfectly conducting spherical shell having a circular aperture and illuminated by a plane (c. w.) electromagnetic wave at symmetrical incidence. This was previously treated by Chang and Senior (1969) by expanding the interior and exterior fields in spherical modes and determining the coefficients by a 'least squares' method. Since their main interest was in the effect of the aperture-cavity combination on the scattering properties of a solid sphere, a program was developed to compute the scattered field, and by taking explicit account of the field behavior close to the edges of the aperture, data were obtained which were in good agreement with experiment.

The program has been modified to permit the calculation of the fields within the cavity, and though it is rather expensive to run, the fields have been computed at selected points inside and on the shell for two aperture half angles

and for $0.5 \leq ka \leq 5.0$, where a is the radius of the cavity. These data are discussed in Chapters 3 and 4.

It is obvious that the analysis would be greatly simplified if the coupling between the cavity and the aperture were wholly or substantially ignored. The aperture and cavity problems could then be treated independently of one another and, having found the field distribution across the aperture when placed in an infinite screen, the determination of the cavity fields would be relatively straightforward. For added generality, certain arbitrary constants could be incorporated into the aperture distribution obtained, which constants could then be chosen to satisfy the boundary conditions at a like number of points in the aperture of the cavity. Unfortunately, all this is easier said than done. The calculation of the aperture fields is by no means a simple problem and this is particularly true if the aperture is not circular and/or the screen is non-planar. Moreover, the manner in which the infinite screen should be chosen, and the effect which the geometry of the screen has on the aperture distribution, are not obvious. It therefore seems logical to approximate this distribution at the outset, and avoid entirely the complexity of the aperture problem.

Two approximations of this type are discussed in Chapter 2. The first of these is appropriate to an electrically large aperture and postulates a field within the aperture identical to the incident field apart from an amplitude scaling factor $\gamma$. The cavity fields are now trivially obtainable and $\gamma$ can be chosen to ensure continuity of a field component at an isolated point of the aperture. The second approximation is for an electrically small aperture where the distribution is dominated by edge effects and can be found by considering the problem of a small aperture in a plane screen. Here again the distribution can be scaled in amplitude, which factor can be chosen as before to incorporate some minimal interaction between the cavity and its aperture. The latter approximation is identical to the one proposed by Enander (1971). Of these two approaches only the first is implemented in this Note and even then the calculation of the scaling

factor in the manner that we have described has not been carried out. Values of $\gamma$ have been determined by fitting the interior field distributions to the exact data computed using the Chang-Senior program, and these are tabulated. Reasonably good fits are obtained.

An approach which is even simpler is to ignore the cavity entirely and to regard the aperture as being in an infinite screen. Using now the aperture distribution appropriate to large or small apertures, the transmitted fields can be trivially computed. The results of these calculations are also compared with the exact data. Not surprisingly the agreement is much poorer than for the earlier approximation.

## 2. Mathematical Considerations

An infinitely thin, perfectly conducting spherical shell having a circular aperture is illuminated by a plane electromagnetic wave at symmetrical incidence. In terms of the spherical polar coordinates $(r, \theta, \phi)$ with origin at the center, the equation of the shell is $r = a$, $\theta_o < \theta \leq \pi$, where $\theta_o$ is the half angle of the aperture (see Fig. 1). The incident field is assumed linearly

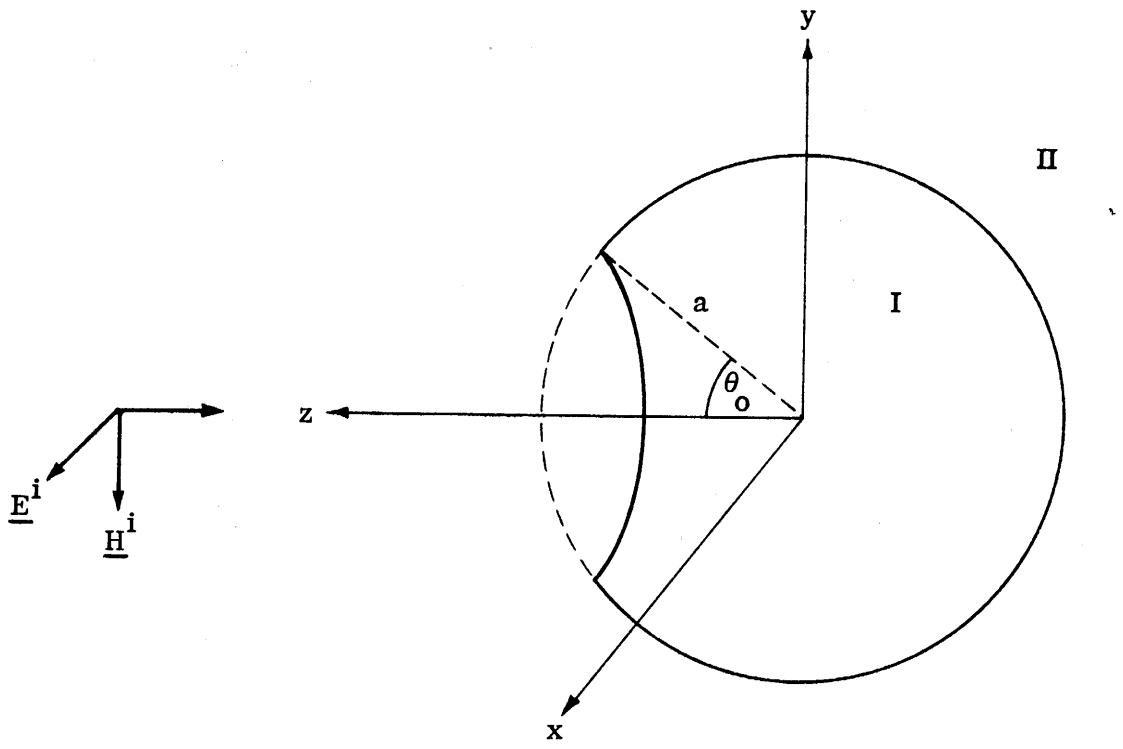


Fig. 1: Spherical shell geometry.

polarised with its electric vector in the x direction and propagates in the negative z direction; we can therefore write

$$\underline{E}^i = \hat{x} e^{jkz} \quad , \quad \underline{H}^i = -\hat{y} Y e^{jkz} \quad , \tag{1}$$

where k is the free space propagation constant, $Y = 1/Z$ is the intrinsic admittance of free space, and a time factor $e^{j\omega t}$ has been suppressed. The task is to find the interior fields as functions of $\theta_o$, ka and position.

2.1 Exact Solution

A natural approach is to introduce the spherical vector wave functions $\underline{M}$ and $\underline{N}$ defined by Stratton (1941). As is well known,

$$\underline{E}^i = \sum_{n=1}^{\infty} j^n \frac{2n+1}{n(n+1)} \left\{ \underline{M}_{o1n}^{(1)} - j \underline{N}_{e1n}^{(1)} \right\} ,$$

$$\underline{H}^i = jY \sum_{n=1}^{\infty} j^n \frac{2n+1}{n(n+1)} \left\{ \underline{N}_{o1n}^{(1)} - j \underline{M}_{e1n}^{(1)} \right\} , \tag{2}$$

where the superscript 1 indicates that the radial dependence is provided by

$$\psi_n(kr) = kr j_n(kr)$$

where $j_n(kr)$ is the spherical Bessel function of order n. The interior field in the region I, $0 \leq \rho \leq a$, can be expanded in a similar manner, but with unknown amplitude coefficients:

$$\underline{E}^I = \sum_{n=1}^{\infty} \left\{ A_n \underline{M}_{o1n}^{(1)} - j B_n \underline{N}_{e1n}^{(1)} \right\} ,$$

$$\underline{H}^I = jY \sum_{n=1}^{\infty} \left\{ A_n \underline{N}_{o1n}^{(1)} - j B_n \underline{M}_{e1n}^{(1)} \right\} , \tag{3}$$

whereas in the exterior region II, $a \leq \rho < \infty$, we have

$$\underline{E}^{II} = \underline{E}^i + \underline{E}^s ,$$

$$\underline{H}^{II} = \underline{H}^i + \underline{H}^s , \tag{4}$$

with the scattered field $\underline{E}^s$, $\underline{H}^s$ having the form

$$\underline{E}^s = \sum_{n=1}^{\infty} \left\{ C_n \underline{M}^{(4)}_{o1n} - jD_n \underline{N}^{(4)}_{e1n} \right\} ,$$

$$\underline{H}^s = jY \sum_{n=1}^{\infty} \left\{ C_n \underline{N}^{(4)}_{o1n} - jD_n \underline{M}^{(4)}_{e1n} \right\} . \qquad (5)$$

From the requirement that this satisfy the radiation condition, $\underline{M}^{(4)}$ and $\underline{N}^{(4)}$ differ from $\underline{M}^{(1)}$ and $\underline{N}^{(1)}$ in having $\psi_n(kr)$ replaced by

$$\xi_n(kr) = kr\, h_n^{(2)}(kr)$$

where $h_n^{(2)}(kr)$ is the spherical Hankel function of the second kind of order n. The unknown coefficients $A_n$, $B_n$, $C_n$ and $D_n$ are to be determined from the boundary conditions that the fields be continuous through the aperture and the tangential components of the electric field vanish on the perfectly conducting shell. Since the shell is thin, there is also the possibility that the edge condition at $\theta = \theta_o$ must be explicitly imposed.

From the continuity of $E_\theta$ and $E_\phi$ through the aperture and the fact that these components are zero on both sides of the shell, it follows that for all $\theta$, $0 \le \theta \le \pi$,

$$E_\theta^I = E_\theta^{II} , \qquad E_\phi^I = E_\phi^{II} \qquad \text{on} \qquad r = a.$$

Application of the orthogonality relations (Bailin and Silver, 1956) for the Legendre functions to the field expansions (2), (3) and (5) then gives

$$C_n \xi_n(ka) = \left\{ A_n - j^n \frac{2n+1}{n(n+1)} \right\} \psi_n(ka) ,$$

$$D_n \xi_n'(ka) = \left\{ B_n - j^n \frac{2n+1}{n(n+1)} \right\} \psi_n'(ka) , \qquad (6)$$

where the prime denotes the derivative with respect to the entire argument.

To complete the specification of the coefficients, it is sufficient to impose the requirements that $E_\theta^{II}$ and $E_\phi^{II}$ vanish on the shell and that $H_\theta$ and $H_\phi$ are continuous through the aperture. If, following Chang and Senior (1969), these conditions are imposed directly, two pairs of infinite series relations involving the $C_n$ and $D_n$ are obtained, the first holding for $\theta_o < \theta \leq \pi$ and the second for $0 \leq \theta < \theta_o$. These equations can be solved by applying weighting factors to each pair and using the method of least square error. Having found the coefficients, Chang and Senior then computed the far bistatic (scattered) field as well as the tangential components of the electric and magnetic field on the outer surface $r = a+0$ of the body.

Unfortunately, the agreement with experimental data was not good. This was attributable to the poor convergence of the series expressions and the marginal accuracy of the numerical scheme as a whole. To improve the accuracy, the formulation was modified to take explicit account of the known field behavior close to the edge of the aperture. Functions representing the edge behavior were expanded in spherical vector wave functions, and this enabled the least squares method to be cast in terms of modified coefficients $c_n$ and $d_n$. Some of the convergence difficulties were now removed and the accuracy of the results obtained was significantly improved. Apart from a few minor changes necessary to reflect the present interest in the interior, rather than the scattered field, the computer program which Chang and Senior developed based on this modified formulation is the one that has been used to generate the 'exact' data included in this Note.

As Chang and Senior noted, the least squares method is only one of several possible approaches to a numerical solution of the problem. One alternative is to construct integral equations for the tangential components of the electric field in the aperture and seek a solution by the moment method.

Although this procedure was originally discarded because of the additional integrations involved, it is of interest to examine the form that these equations take.

Let us assume that in the aperture, $0 \leq \theta < \theta_o$,

$$E_\theta = f(\theta) \cos\phi \quad , \quad E_\phi = g(\theta) \sin\phi \quad . \tag{7}$$

Since $E_\theta^I = E_\phi^I = 0$ for $\theta_o < \theta \leq \pi$, application of the orthogonality relations for the Legendre functions to the series expressions for these components gives

$$A_n = \frac{2n+1}{2n^2(n+1)^2} \frac{ka}{\psi_n(ka)} \int_0^{\theta_o} \left\{ f(\theta) \frac{P_n^1(\cos\theta)}{\sin\theta} - g(\theta) \frac{\partial}{\partial\theta} P_n^1(\cos\theta) \right\} \sin\theta \, d\theta$$

$$B_n = j \frac{2n+1}{2n^2(n+1)^2} \frac{ka}{\psi_n'(ka)} \int_0^{\theta_o} \left\{ f(\theta) \frac{\partial}{\partial\theta} P_n^1(\cos\theta) - g(\theta) \frac{P_n^1(\cos\theta)}{\sin\theta} \right\} \sin\theta \, d\theta \tag{8}$$

and it only remains to impose the requirement that $H_\theta$ and $H_\phi$ are continuous through the aperture. This is a relatively straightforward task, and using the eqs. (6) and the Wronskian relation

$$\psi_n(ka)\xi_n'(ka) - \psi_n'(ka)\xi_n(ka) = -j \quad ,$$

we find

$$\sum_{n=1}^{\infty} \left\{ \frac{A_n}{\xi_n(ka)} \frac{\partial}{\partial\theta} P_n^1(\cos\theta) - j \frac{B_n}{\xi_n'(ka)} \frac{P_n^1(\cos\theta)}{\sin\theta} \right\} = -ka\, T_1(\theta)$$

$$\sum_{n=1}^{\infty} \left\{ \frac{A_n}{\xi_n(ka)} \frac{P_n^1(\cos\theta)}{\sin\theta} - j \frac{B_n}{\xi_n'(ka)} \frac{\partial}{\partial\theta} P_n^1(\cos\theta) \right\} = -ka\, T_2(\theta) \tag{9}$$

valid for $0 \leq \theta < \theta_o$, where

$$T_1(\theta) = \frac{1}{ka} \sum_{n=1}^{\infty} j^{n+1} \frac{2n+1}{n(n+1)} \left\{ \frac{1}{\xi_n'(ka)} \frac{P_n^1(\cos\theta)}{\sin\theta} + \frac{j}{\xi_n(ka)} \frac{\partial}{\partial\theta} P_n^1(\cos\theta) \right\}$$

$$T_2(\theta) = \frac{1}{ka} \sum_{n=1}^{\infty} j^{n+1} \frac{2n+1}{n(n+1)} \left\{ \frac{1}{\xi_n'(ka)} \frac{\partial}{\partial\theta} P_n^1(\cos\theta) + \frac{j}{\xi_n(ka)} \frac{P_n^1(\cos\theta)}{\sin\theta} \right\} \tag{10}$$

are proportional to the tangential components of $H_\theta$ and $H_\phi$ respectively on a complete perfectly conducting sphere illuminated by the plane wave (1). Substitution of (8) into (9) now leads to two coupled integral equations for the unknown aperture fields f and g, viz

$$\int_0^{\theta_o} \left\{ f(\alpha)\, K_1(\alpha, \theta) + g(\alpha)\, K_2(\alpha, \theta) \right\} d\alpha = T_1(\theta)$$

$$\int_0^{\theta_o} \left\{ f(\alpha)\, K_3(\alpha, \theta) + g(\alpha)\, K_4(\alpha, \theta) \right\} d\alpha = T_2(\theta) \tag{11}$$

where

$$K_1(\alpha, \theta) = -\sin\alpha \sum_{n=1}^{\infty} \frac{2n+1}{2n^2(n+1)^2} \left\{ \frac{1}{\psi_n \xi_n} \frac{\partial}{\partial\theta} P_n^1(\cos\theta) \frac{P_n^1(\cos\alpha)}{\sin\alpha} + \frac{1}{\psi_n' \xi_n'} \frac{P_n^1(\cos\theta)}{\sin\theta} \frac{\partial}{\partial\alpha} P_n^1(\cos\alpha) \right\}$$

$$K_2(\alpha, \theta) = \sin\alpha \sum_{n=1}^{\infty} \frac{2n+1}{2n^2(n+1)^2} \left\{ \frac{1}{\psi_n \xi_n} \frac{\partial}{\partial\theta} P_n^1(\cos\theta) \frac{\partial}{\partial\theta} P_n^1(\cos\alpha) + \frac{1}{\psi_n' \xi_n'} \frac{P_n^1(\cos\theta)}{\sin\theta} \frac{P_n^1(\cos\alpha)}{\sin\alpha} \right\}$$

$$K_3(\alpha, \theta) = -\sin\alpha \sum_{n=1}^{\infty} \frac{2n+1}{2n^2(n+1)^2} \left\{ \frac{1}{\psi_n \xi_n} \frac{P_n^1(\cos\theta)}{\sin\theta} \frac{P_n^1(\cos\alpha)}{\sin\alpha} + \frac{1}{\psi_n' \xi_n'} \frac{\partial}{\partial\theta} P_n^1(\cos\theta) \frac{\partial}{\partial\alpha} P_n^1(\cos\alpha) \right\}$$

$$K_4(\alpha,\theta) = \sin\alpha \sum_{n=1}^{\infty} \frac{2n+1}{2n^2(n+1)^2} \left\{ \frac{1}{\psi_n \xi_n} \frac{P_n^1(\cos\theta)}{\sin\theta} \frac{\partial}{\partial\alpha} P_n^1(\cos\alpha) + \frac{1}{\psi_n' \xi_n'} \frac{\partial}{\partial\theta} P_n^1(\cos\theta) \frac{P_n^1(\cos\alpha)}{\sin\alpha} \right\} .$$

In principle at least, the eqs. (11) could be solved by the moment method. Having found f and g, the $A_n$ and $B_n$ could then be computed from the eqs. (8) and the interior (transmitted) and exterior (scattered) fields determined. The process would involve an integration followed by the summation of an infinite series for either field, but to our knowledge this procedure has not yet been used. Based on our experience with the least squares method, it would appear desirable to build the explicit edge behavior into the functions f and g in order that the accuracy of the resulting $A_n$ and $B_n$, particularly for large n, is sufficient for evaluating the infinite series expressions for the fields.

## 2.2 Approximate Solutions

The main source of difficulty in the present problem is the coupling through the aperture between the exterior and the cavity, and were it possible to separate these two parts, the analysis could be greatly simplified. To carry out the separation is, of course, an approximation, but this would permit a variety of less complicated 'solutions' to be developed. Though their validity is limited, such approximate methods of solution are virtually our only hope for predicting the field penetration into cavities of complex shape. It is therefore of interest to use the exact data obtained for the present geometry to assess the accuracy of these approximate solutions.

The first two methods to be considered are based on approximations to the aperture field. If the aperture is electrically large ($ka \sin\theta_o \gg 1$) and the influence of the cavity can be ignored, the Kirchoff approximation in which $f(\theta)$ and $g(\theta)$ are given the values appropriate to the incident field would be a natural one to employ. In practice, the cavity will certainly affect the aperture field, particularly at frequencies close to the resonant frequencies of the cavity, but

if it is assumed that the main effect is to change the amplitude of this field whilst leaving its form unaltered, we are led to the following approximation:

$$f(\theta) = \gamma \cos\theta \, e^{jka\cos\theta}$$
$$g(\theta) = -\gamma \, e^{jka\cos\theta} \qquad (12)$$

where $\gamma$ is a factor to be determined. Substitution into the eqs. (8) enables the mode coefficients $A_n$ and $B_n$ to be found, and the interior field can then be computed from the series expressions (3).

Such a solution is, of course, approximate since the formulae (12) for f and g violate the integral equations (11). The resulting magnetic field components $H_\theta$ and $H_\phi$ are not then continuous through the aperture, but by choosing $\gamma$ appropriately, we can force continuity at one point at least. If the point selected is the midpoint, $\theta = 0$, of the aperture, both $H_\theta$ and $H_\phi$ can be made continuous there. However, the poor convergence of the series expressions for the kernels $K_i(\alpha, \theta)$, $i = 1, \ldots, 4$ (or, equivalently, of the series on the left hand sides of the eqs. (9)) makes it desirable to choose $\theta$ as large as possible, i.e., $\theta = \theta_o$, notwithstanding the actual (but excluded) singularity of the aperture fields at the edge. We then have the choice of matching $H_\theta$ or $H_\phi$, but can no longer match both using a single value of $\gamma$. Although such a procedure for finding $\gamma$ has not been implemented, the cavity fields predicted by the approximation (12) have been computed and compared with the exact results. Selected data are presented in Chapter 3 and the values of $\gamma$ which produce the 'best' fit to the exact results are given there.

Whereas the approximation (12) has most merit if $ka \sin\theta_o \gg 1$ (implying $ka \gg 1$, a fortiori), a similar approach is possible for electrically small apertures. Edge effects are now dominant and provide a basis for approximating the functions f and g. If we again assume that the role played by the cavity is primarily to scale in amplitude the fields which would otherwise exist if the cavity were not there, we are led to the approximation

$$f(\theta) = \gamma \left\{ 2(\cos\theta - \cos\theta_o) \right\}^{1/2}$$

$$g(\theta) = -\gamma \left[ \left\{ 2(\cos\theta - \cos\theta_o) \right\}^{1/2} + \frac{1}{2} \sin^2\theta \left\{ 2(\cos\theta - \cos\theta_o) \right\}^{-1/2} \right] , \qquad (13)$$

where $\gamma$ is a scaling factor which can be chosen in the same manner as before. The approximation (13) has been used by Enander (1971), but no data were presented. The approach has obvious similarities to Bethe's theory of small holes and, apart from the factor $\gamma$, the aperture distribution (13) is just that which is appropriate to a small circular aperture in a plane screen. As regards the interior fields, Bethe (1944) simulates the effect of the aperture by electric and magnetic dipoles placed on the inside of the shell, but since the aperture is now lumped at the single point $\theta = 0$, it is no longer obvious how a factor $\gamma$ could be determined if one were included in the dipole strengths.

With each of the above approximations, the aperture is part of the cavity shell, but the entire influence of the cavity on the aperture field is embodied in the factor $\gamma$. This is certainly only a minimal inclusion of the true effect that the cavity will have. In practice, the resonant properties of the cavity may affect the aperture field in form, as well as amplitude and phase, and though the factor $\gamma$ <u>can</u> be chosen to provide a reasonable simulation of the interior fields even close to the resonant frequencies (see Chapter 3), such a choice requires a knowledge of the exact solution. If $\gamma$ is determined by matching the tangential magnetic fields at a designated point, it is by no means certain that the resulting cavity fields will reproduce the true resonance properties, and it seems probable that the data will have most accuracy at frequencies well away from resonance for cavities that are electrically large ($ka \gg 1$).

We can reduce still further the consideration of the cavity by ignoring it entirely and we are then left with the problem of a spherical cap aperture. By assuming this to be part of an infinite screen, trivial approximations to the

transmitted field can be developed that are analogous to those examined above and are appropriate to apertures for which $ka \sin\theta_o \gg 1$ or $ka \sin\theta_o \ll 1$. The results are meaningful only for large cavities ($ka \gg 1$) at points which would lie in their interior.

The geometry for the electrically large aperture is illustrated in Fig. 2.

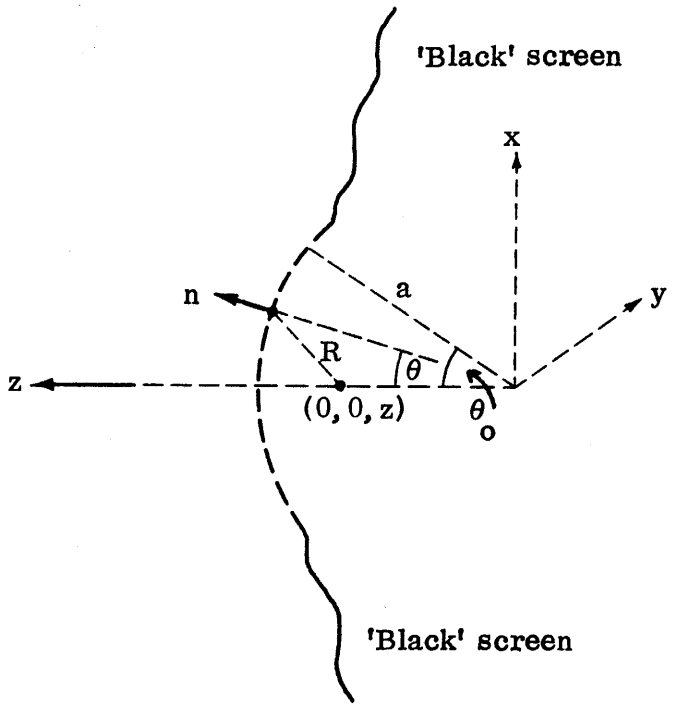


Fig. 2: Geometry for the large aperture approximation C.

At points to the right of the aperture, the fields can be obtained from the electric and magnetic Hertz vectors

$$\underline{\pi}^e(\underline{r}) = -\frac{jZ}{4\pi k}\int \hat{n} \wedge \underline{H}\, \Phi\, dS \qquad (14)$$

$$\underline{\pi}^{m}(\underline{r}) = \frac{jY}{4\pi k}\int \hat{n}\wedge\underline{E}\,\Phi\,dS \tag{14}$$

where $\Phi$ is the free space Green's function, $\Phi = \frac{e^{-jkR}}{R}$, and the integration is carried out over the right hand side of the screen and aperture. If the Kirchoff approximation is now made, i.e., the screen is assumed 'black' (so that $\hat{n}\wedge\underline{H} = \hat{n}\wedge\underline{E} = 0$ there) and the aperture field is taken to be the undistorted incident field, the eqs. (14) reduce to

$$\begin{aligned}\underline{\pi}^{e}(\underline{r}) &= -\frac{jZ}{4\pi k}\int_{A} \hat{n}\wedge\underline{H}^{i}\,\Phi\,dS \\ \underline{\pi}^{m}(\underline{r}) &= \frac{jY}{4\pi k}\int_{A} \hat{n}\wedge\underline{E}^{i}\,\Phi\,dS\end{aligned} \tag{15}$$

where A is the aperture. These are explicit integrals in which the $\phi$ integration can be carried out immediately and from which an expression for the transmitted (interior) field then follows. If, for simplicity, attention is confined to the electric field at points on the symmetry axis of the aperture, it is found that

$$E_x(z) = \frac{a^2}{2}\int_0^{\theta_o}\left\{jkR\cos\theta + (a - z\cos\theta)\left(jk+\frac{1}{R}\right)\right\}e^{jk(a\cos\theta - R)}\,\frac{\sin\theta\,d\theta}{R^2} \tag{16}$$

$$E_y(z) = E_z(z) = 0$$

where

$$R = \left\{a^2 + z^2 - 2az\cos\theta\right\}^{1/2}.$$

It is then obvious that $H_x(z) = H_z(z) = 0$ with $H_y(z) = -YE_x(z)$. These formulae are meaningful only if $|z| < a$ and the results of computations based on eq. (16)

are compared with the exact data in Chapter 3.

The analysis for an electrically small aperture is even more straightforward. By taking the screen S to be a perfectly conducting (planar) sheet whose circular aperture is illuminated by the plane wave (1) at normal incidence, the field in the region to the right can be attributed to a magnetic dipole of moment

$$\underline{m} = \frac{16}{3} Y (a \sin\theta_o)^3 e^{jka} \hat{y}$$

(Bethe, 1944) located at the center of the aperture. The resulting electric field is

$$\underline{E} = -\frac{4}{3\pi} (ka \sin\theta_o)^3 \frac{e^{jk(a-R')}}{kR'} \hat{R}' \wedge \underline{m}$$

where $\underline{R}' = (R', \theta', \phi)$ is the position vector of the point $\underline{r} = (r, \theta, \phi)$ of observation relative to an origin at the dipole, and hence

$$\underline{E} = -\frac{4}{3\pi} (ka \sin\theta_o)^3 \frac{e^{jk(a-R')}}{kR'} (\hat{x} \cos\theta' + \hat{z} \sin\theta' \cos\phi) \qquad (17)$$

with

$$R' = \left\{ a^2 + r^2 - 2ar\cos\theta \right\}^{1/2}$$

$$\sin\theta' = \frac{r}{R'} \sin\theta \quad .$$

It is evident that the approximations (16) and (17) are much cruder than the ones considered earlier and since they ignore completely the presence of the cavity, there is no possibility of observing resonance effects. At best their utility is limited to points within, and away from the walls of, electrically large cavities.

## 3. Computed Data

The computer program developed by Chang and Senior (1969) was modified to permit the calculation of the interior (cavity) fields and to make it more efficient for our purposes, and was then run for a variety of parameter combinations. Nineteen frequencies were considered, corresponding to ka = 0.5 (0.25) 5.0, for each of two aperture half-angles: $\theta_o = 10^o$ (aperture radius = 0.174 a) and $\theta_o = 30^o$ (radius = 0.5 a). The output consisted of the aperture functions f and g (see eqs. (7)) as functions of $\theta$ in increments of $1^o$, and the interior fields at selected points within the cavity. These points were chosen to yield the maximum amount of information for a reasonable expenditure of computer time, and comprised nine equally spaced (a/4 apart) points along the z axis from the aperture to the rear of the cavity and a similar set of points in a transverse direction along the line $\theta = 90^o$, $\phi = 90^o$. Since the fields on the latter line were found to display the same types of variation as those on the main diameter (i.e., the z axis), the data that are presented are for the main diameter only.

The nature of the aperture field is illustrated in Figs. 3 and 4 where $|f(\theta)|$ and $|g(\theta)|$ are plotted as functions of $\theta$ for $\theta_o = 10^o$ and $30^o$ with ka = 2.5. As required, f is infinite at the aperture edges, and the average levels of both $|f|$ and $|g|$ are greater for the larger $\theta_o$. Such behavior is typical of all frequencies including resonant ones, and the frequency for which ka = 2.5 is just short of the lowest resonance, ka = 2.75, of a spherical cavity, corresponding to the first zero of $\psi_1'(ka)$. This is a magnetic mode resonance, is the next higher one (at ka = 3.87, corresponding to the first zero of $\psi_2'(ka)$), but the third is an electric mode resonance occuring at ka = 4.49 and corresponding to the first zero of $\psi_1(ka)$.

Curves showing the variation of the electric and magnetic field amplitudes along the main diameter of the cavity are given in Figs. 5 through 24. Of the 19 frequencies for which data were obtained, only 5 have been selected for presenta-

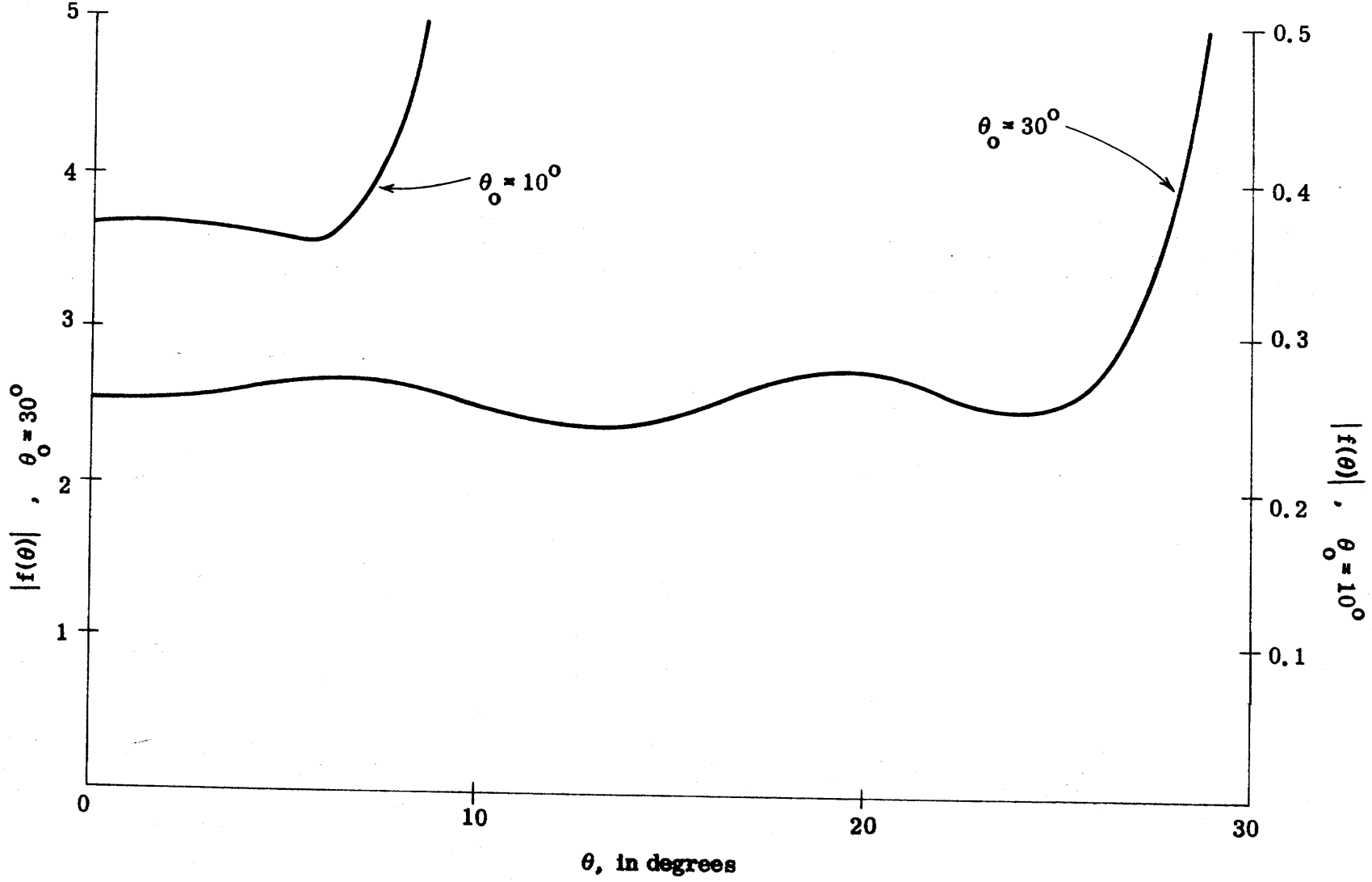


Fig. 3: The amplitude of $E_\theta$ across the aperture for ka = 2.5.

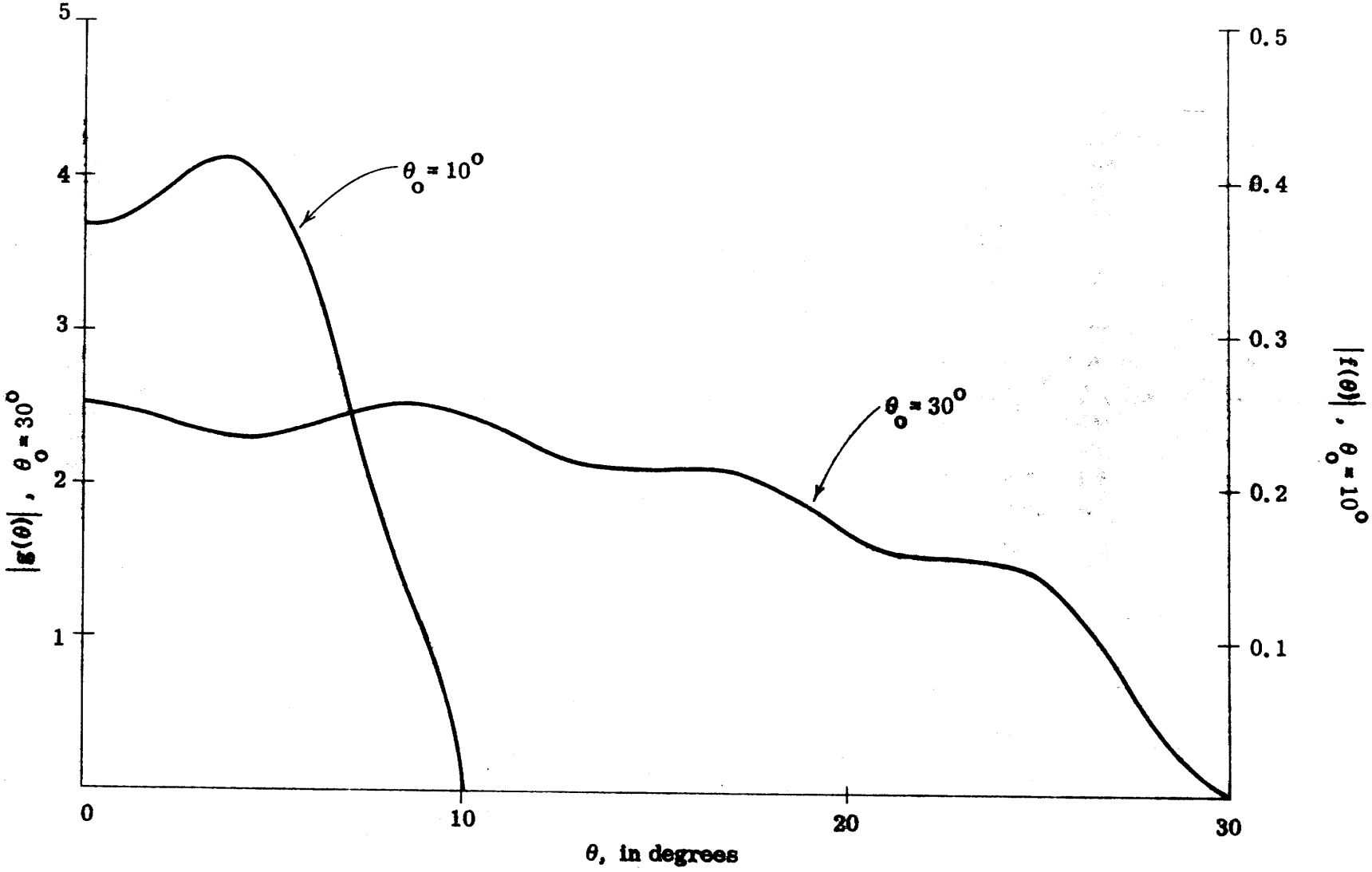


Fig. 4: The amplitude of $E_\phi$ across the aperture for ka = 2.5.

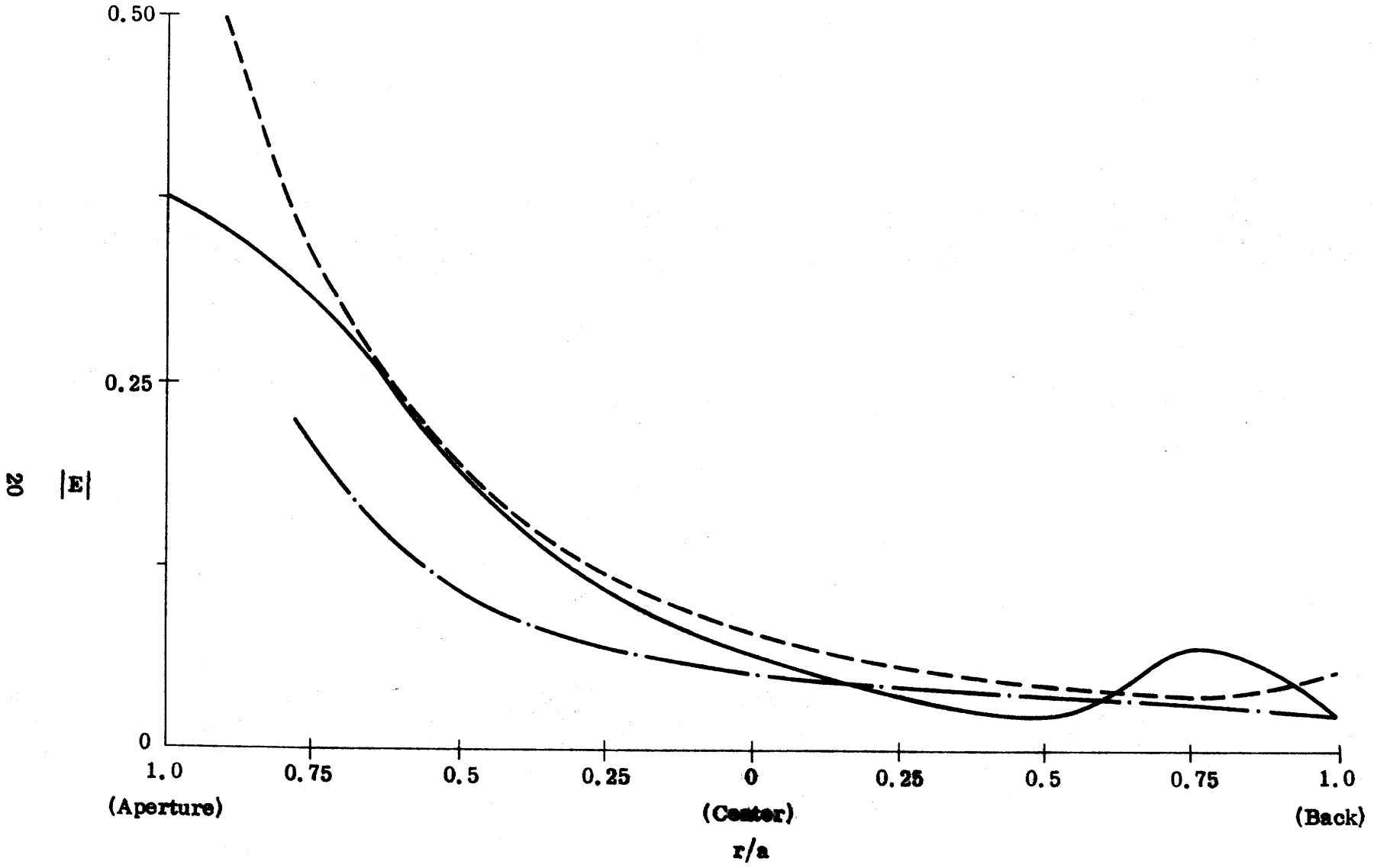


Fig. 5: Amplitude of the electric field along the main diameter for ka = 1.0, $\theta_o = 30^o$: exact (——), approx. A with $\gamma = 0.7$ (– – –), approx. D. (— · —).

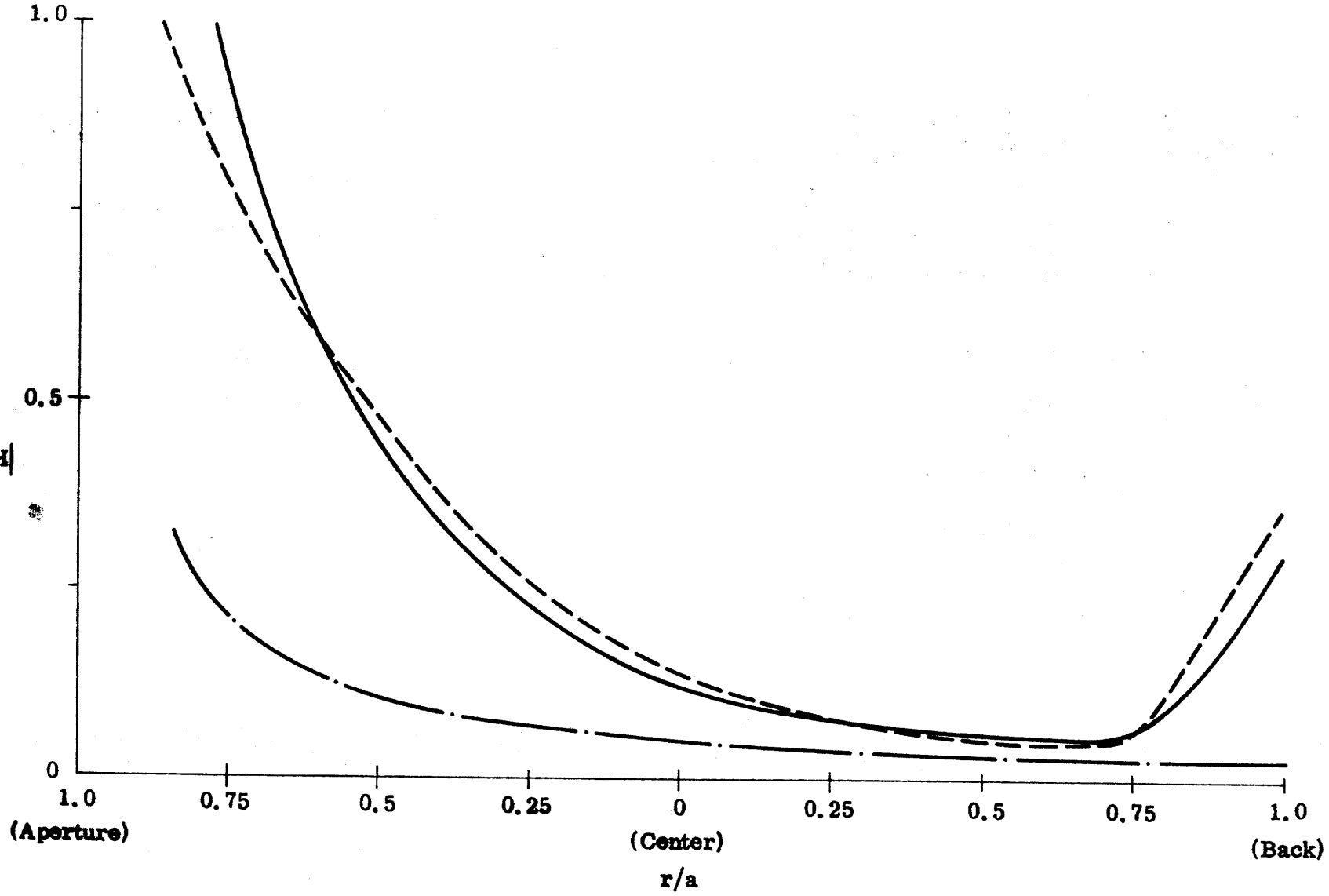


Fig. 6: Amplitude of the magnetic field along the main diameter for ka = 1.0, $\theta_o = 30^o$: exact (——), approx. A with $\gamma = 0.7$ (– – –), approx. D (— · —).

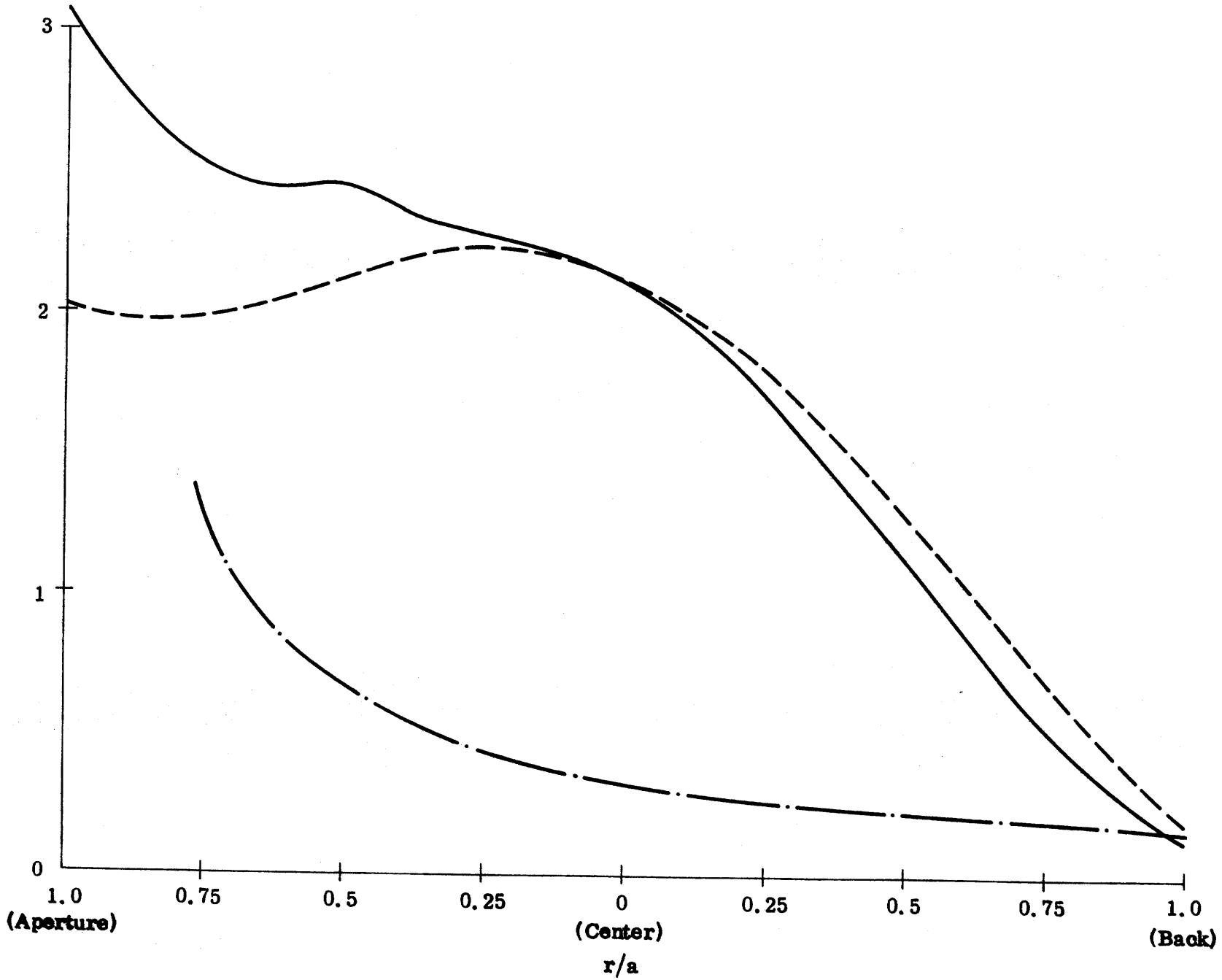


Fig. 7: Amplitude of the electric field along the main diameter for ka = 2.5, $\theta_o = 30^o$: exact (——), approx. A with $\gamma = 2.5$ (– – –), approx. D (— . —).

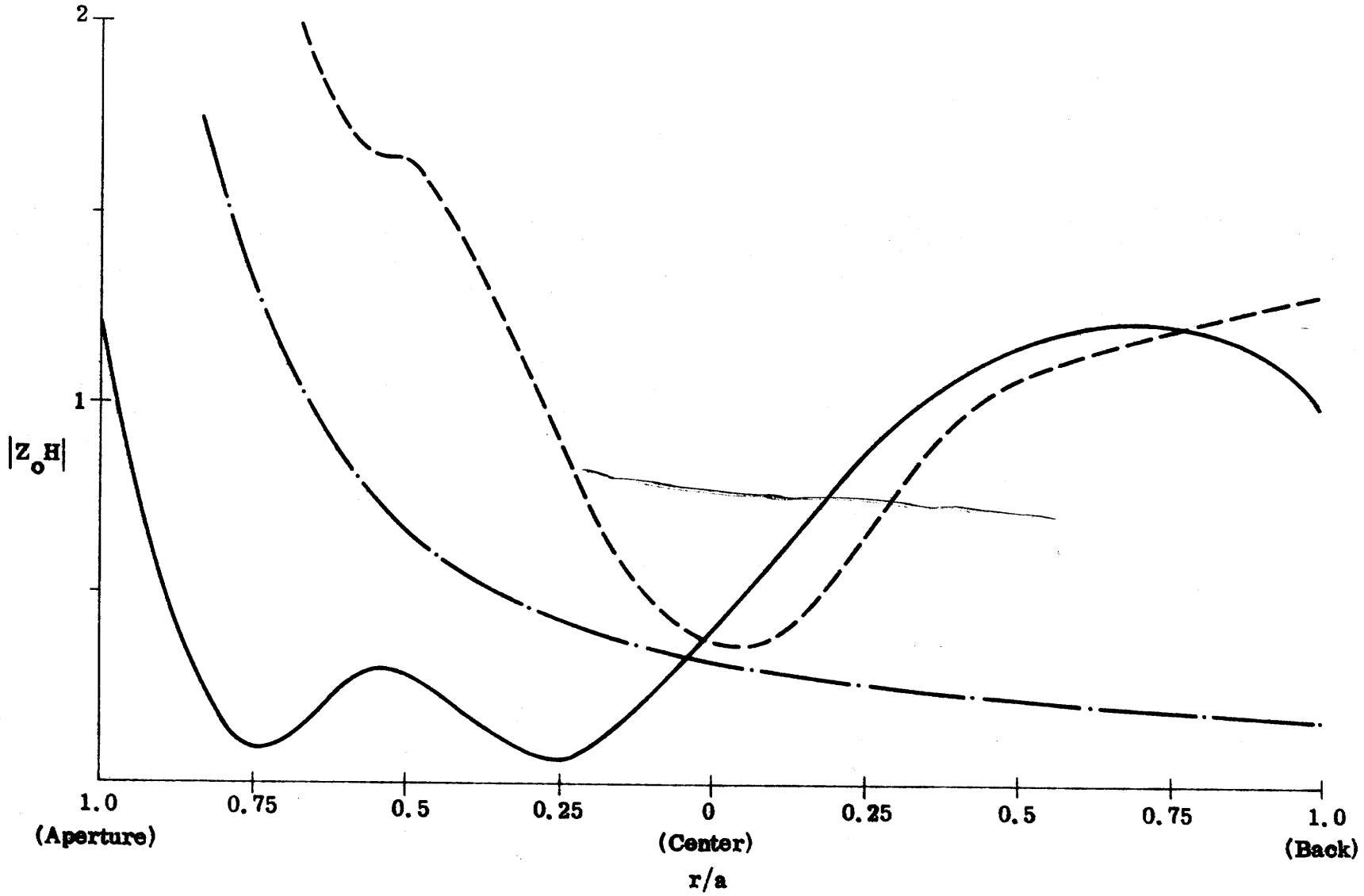


Fig. 8: Amplitude of the magnetic field along the main diameter for ka = 2.5, $\theta_o = 30^o$: exact (——), approx. A with $\gamma = 2.5$ (——), approx. D (— · —).

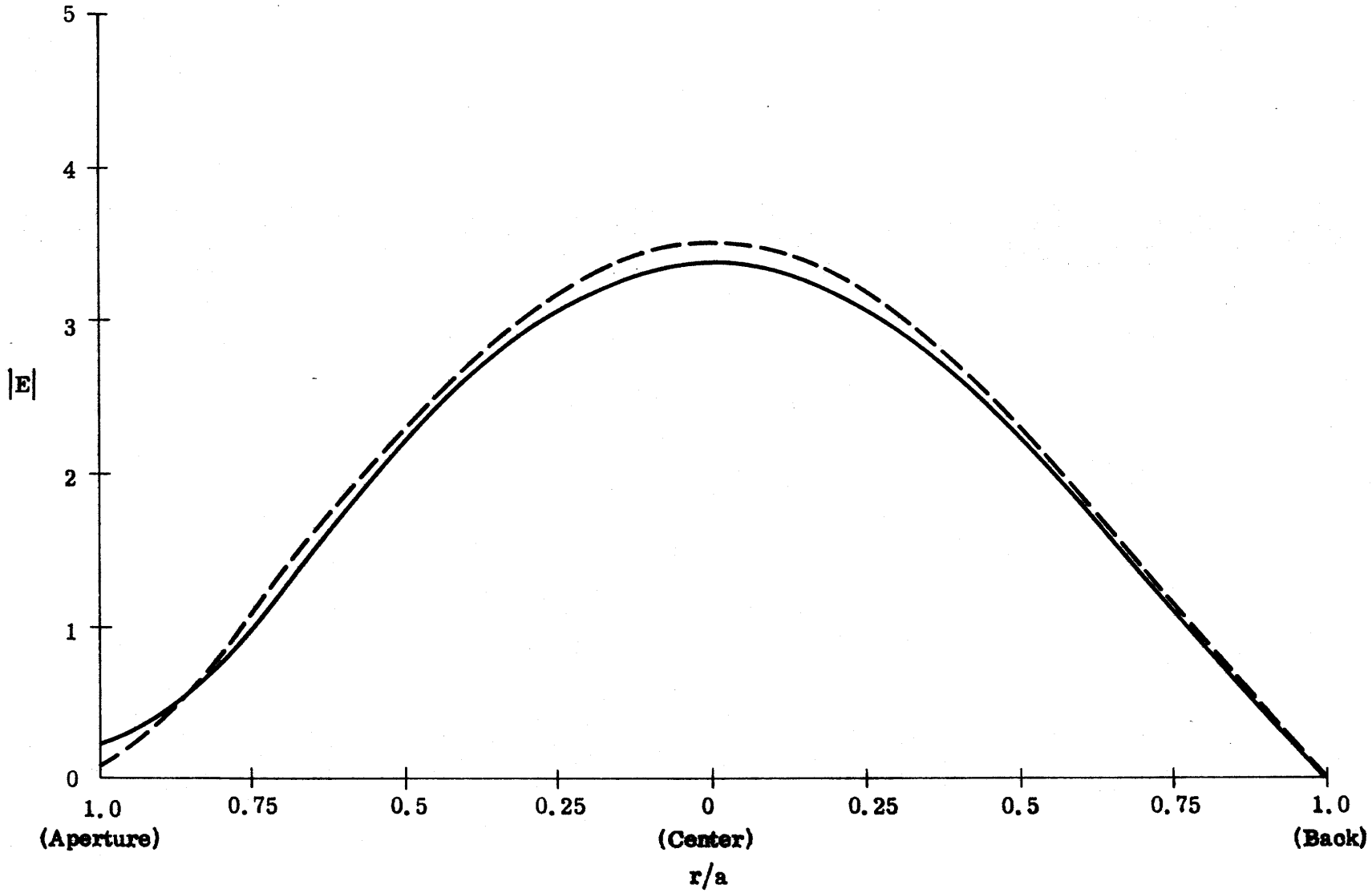


Fig. 9: Amplitude of the electric field along the main diameter for ka = 2.75, $\theta_o = 30^o$: exact (——), approx. A with $\gamma = 0.1$ (– – –).

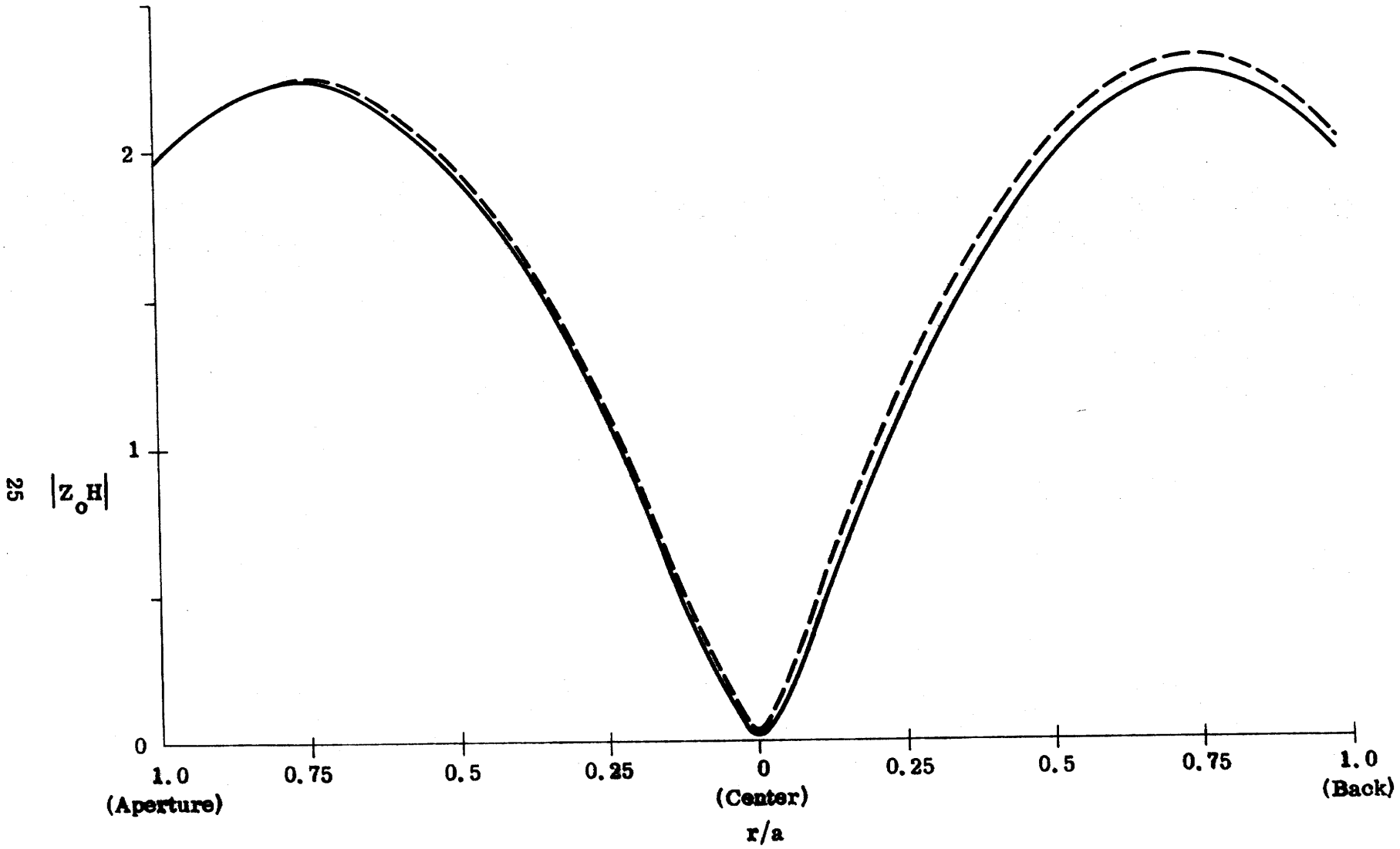


Fig. 10: Amplitude of the magnetic field along the main diameter for ka = 2.75, $\theta_o = 30^o$: exact (——), approx. A with $\gamma = 0.1$ (– – –).

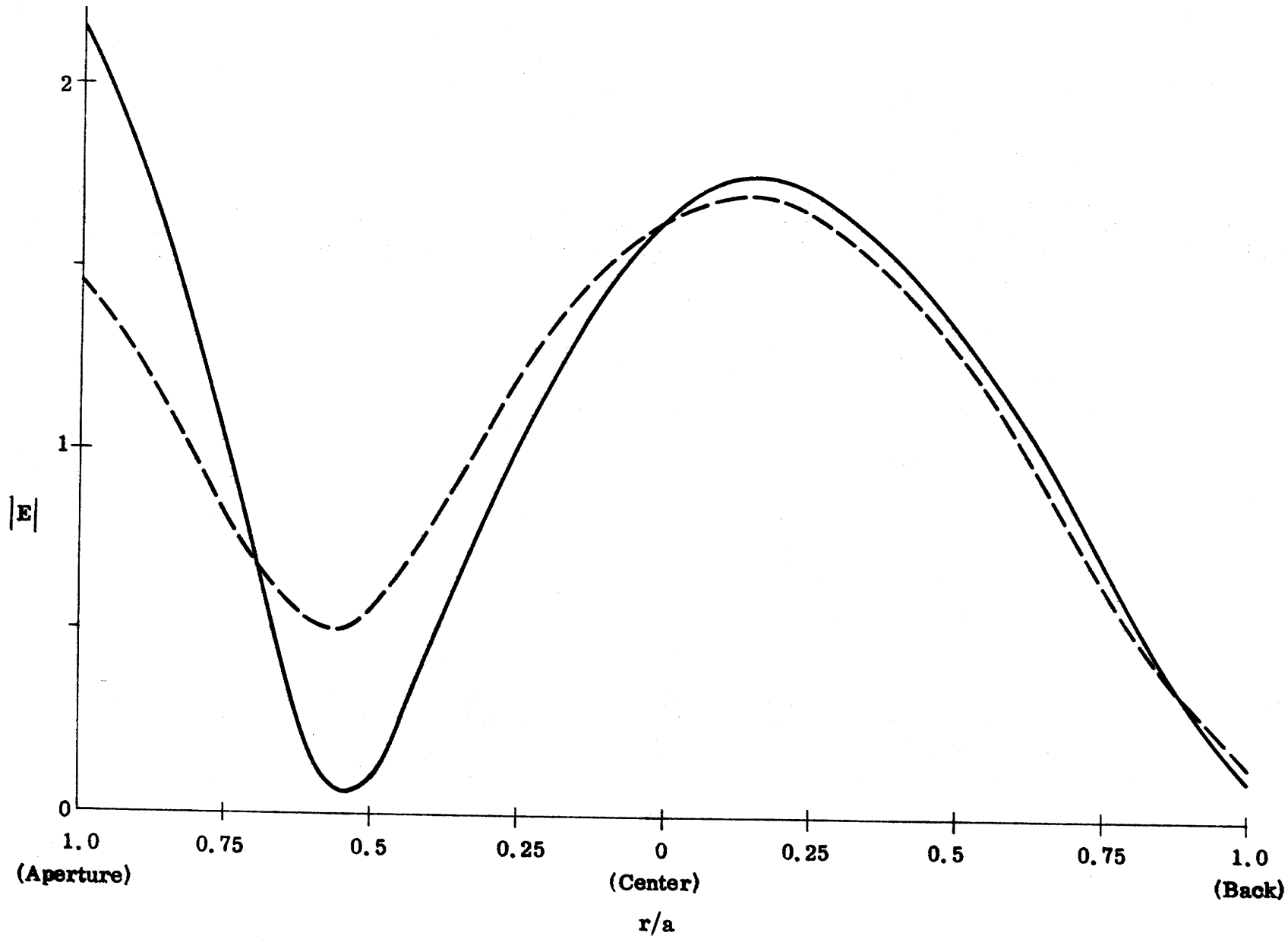


Fig. 11: Amplitude of the electric field along the main diameter for ka = 3.0, $\theta_o = 30^o$: exact (——), approx. A with $\gamma = 1.8$ (– – –).

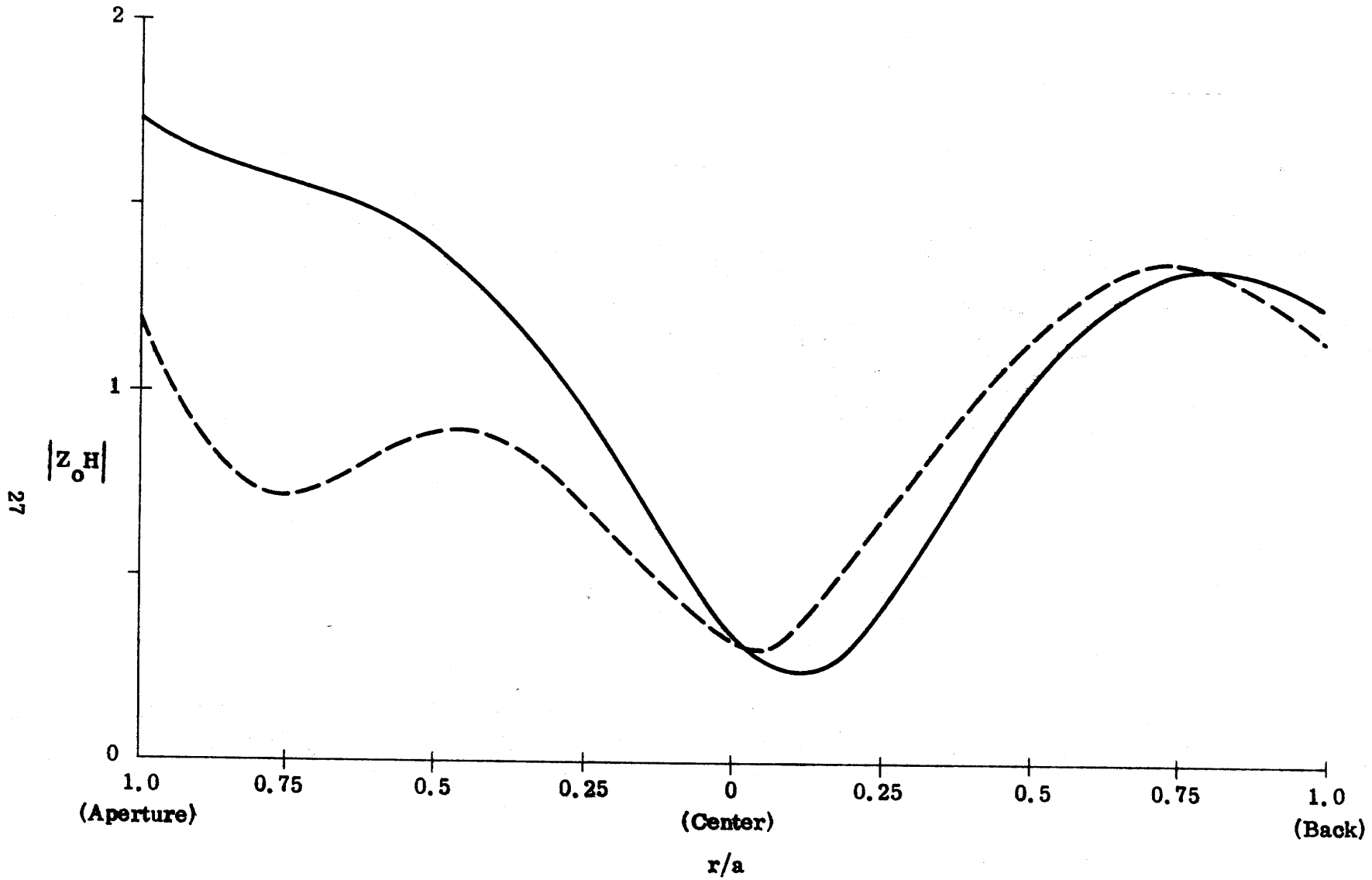


Fig. 12: Amplitude of the magnetic field along the main diameter for ka = 3.0, $\theta_o = 30^o$: exact (——), approx. A with $\gamma = 1.8$ (– – –).

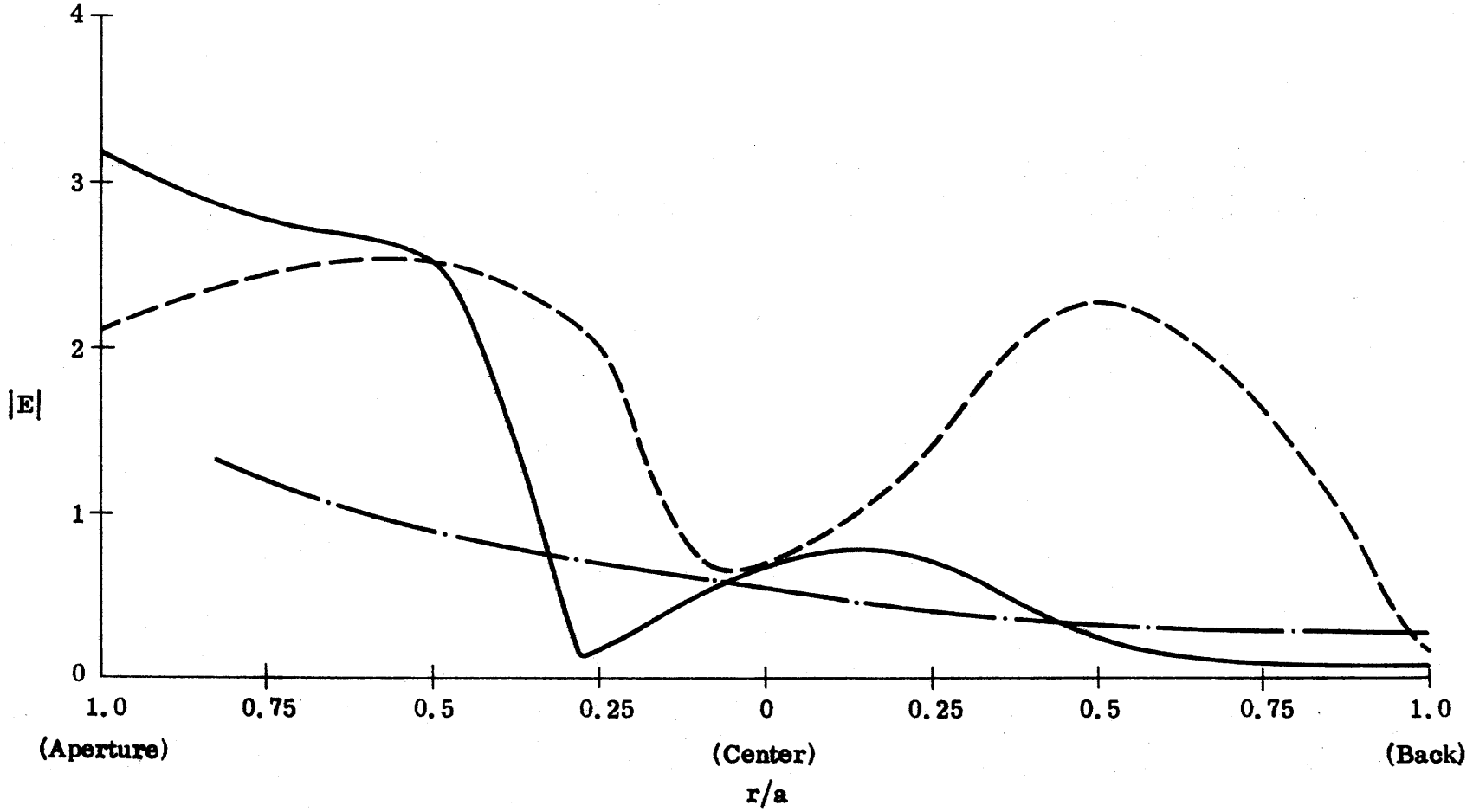


Fig. 13: Amplitude of the electric field along the main diameter for $ka = 4.25$, $\theta_o = 30^o$: exact (——), approx. A with $\gamma = 2.6$ (– – –), approx. C (— · —).

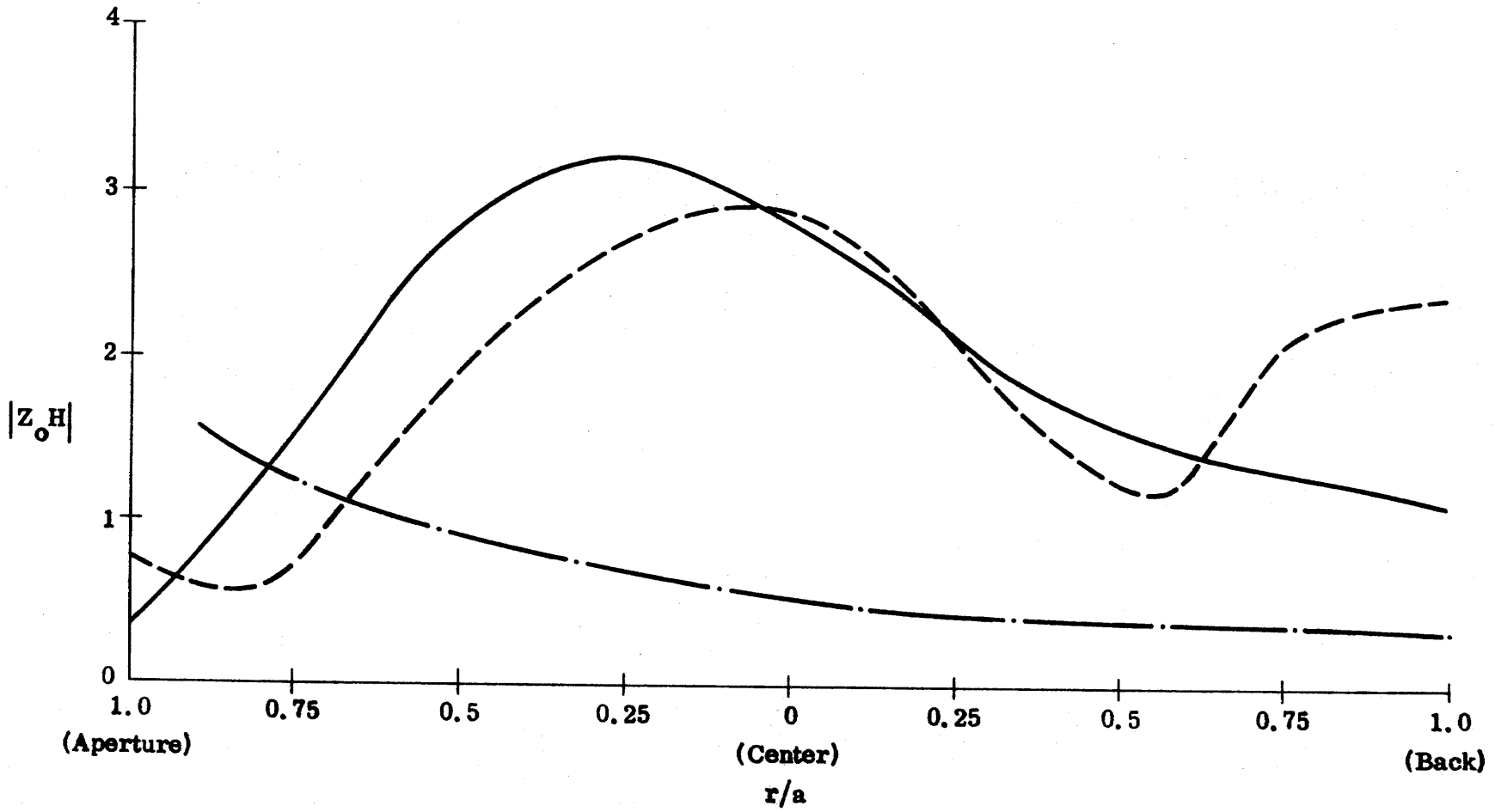


Fig. 14: Amplitude of the magnetic field along the main diameter for ka = 4.25, $\theta_o = 30^o$: exact (——), approx. A with $\gamma = 2.6$ (– – –), approx. C (— · —).

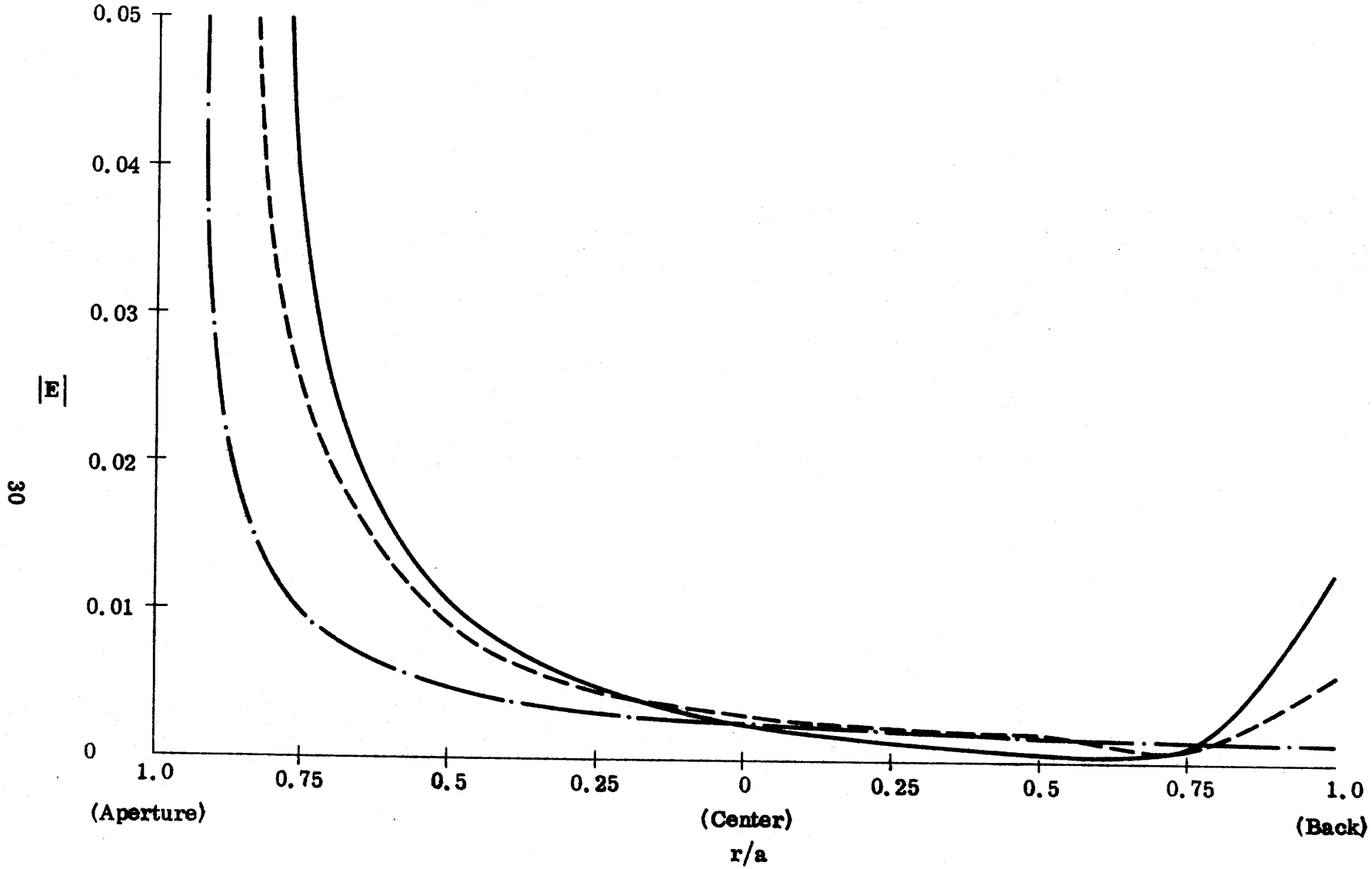


Fig. 15: Amplitude of the electric field along the main diameter for ka = 1.0, $\theta_o = 10^o$: exact (——), approx. A with $\gamma = 0.2$ (——), approx. D (—·—).

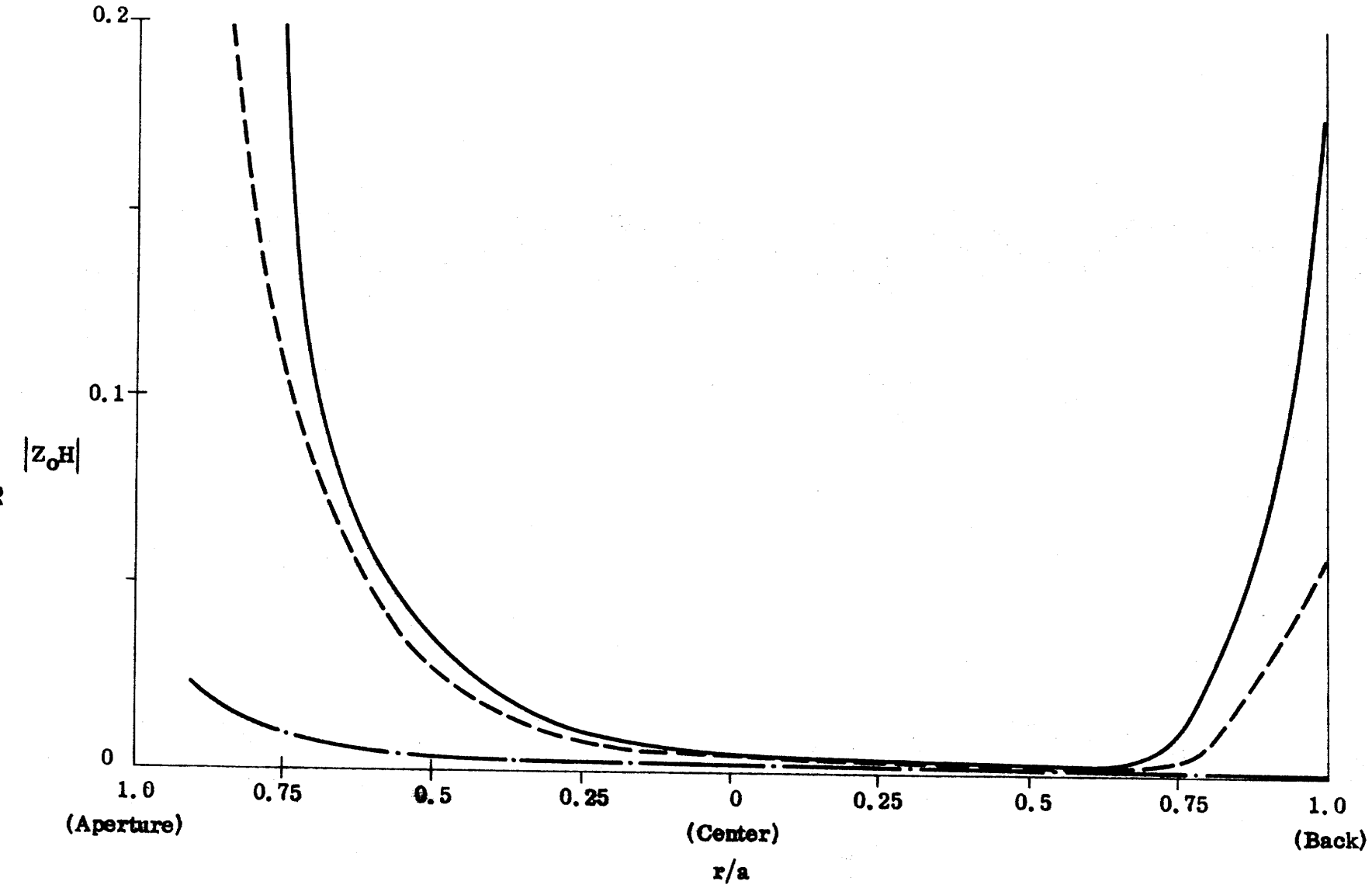


Fig. 16: Amplitude of the magnetic field along the main diameter for $ka = 1.0$, $\theta_0 = 10^\circ$: exact (——), approx. A with $\gamma = 0.2$ (——), approx. D (— · —).

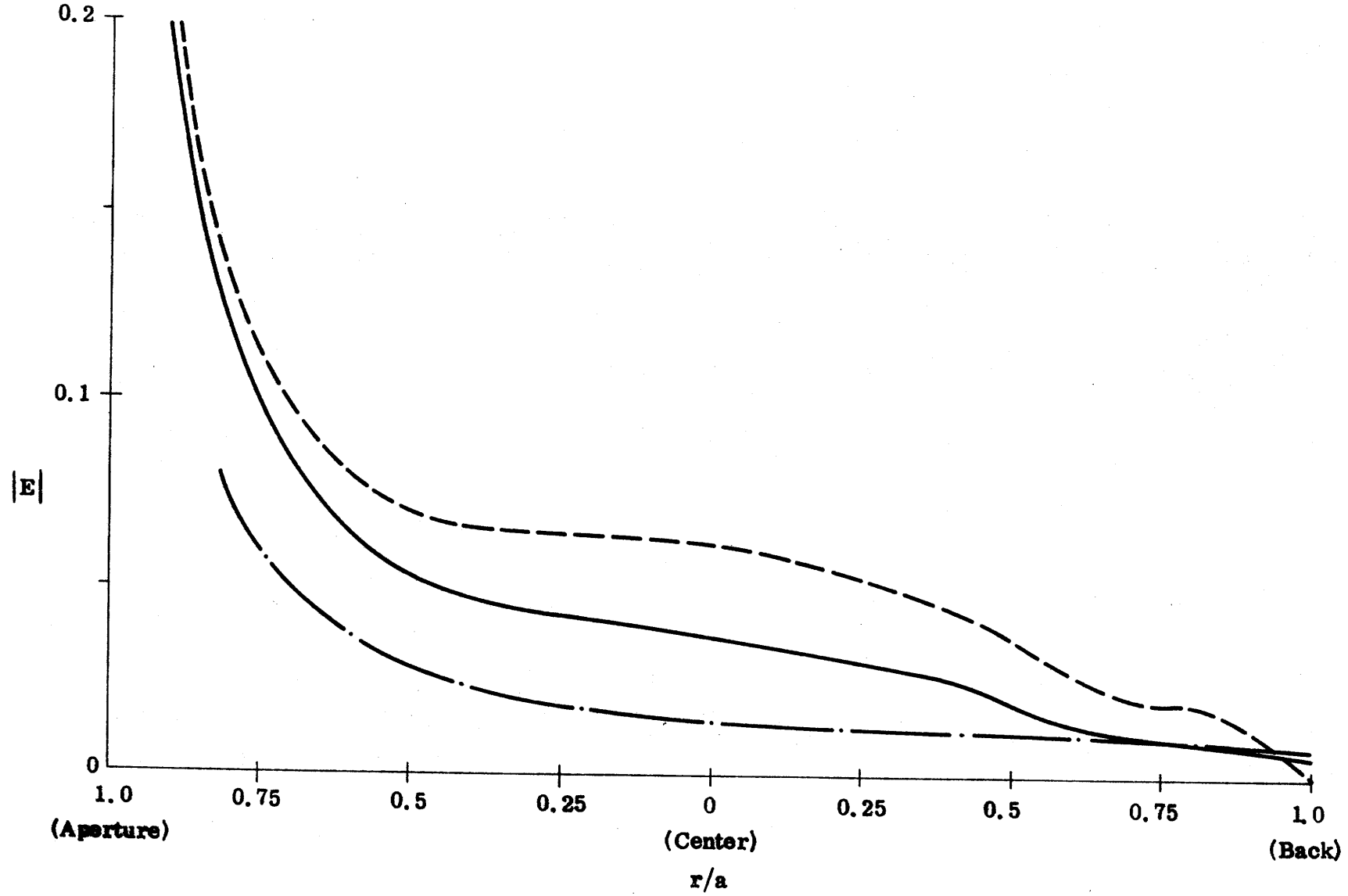


Fig. 17: Amplitude of the electric field along the main diameter for ka = 2.5, $\theta_o = 10^o$: exact (——), approx. A with $\gamma = 0.6$ (– – –), approx. D (— · —).

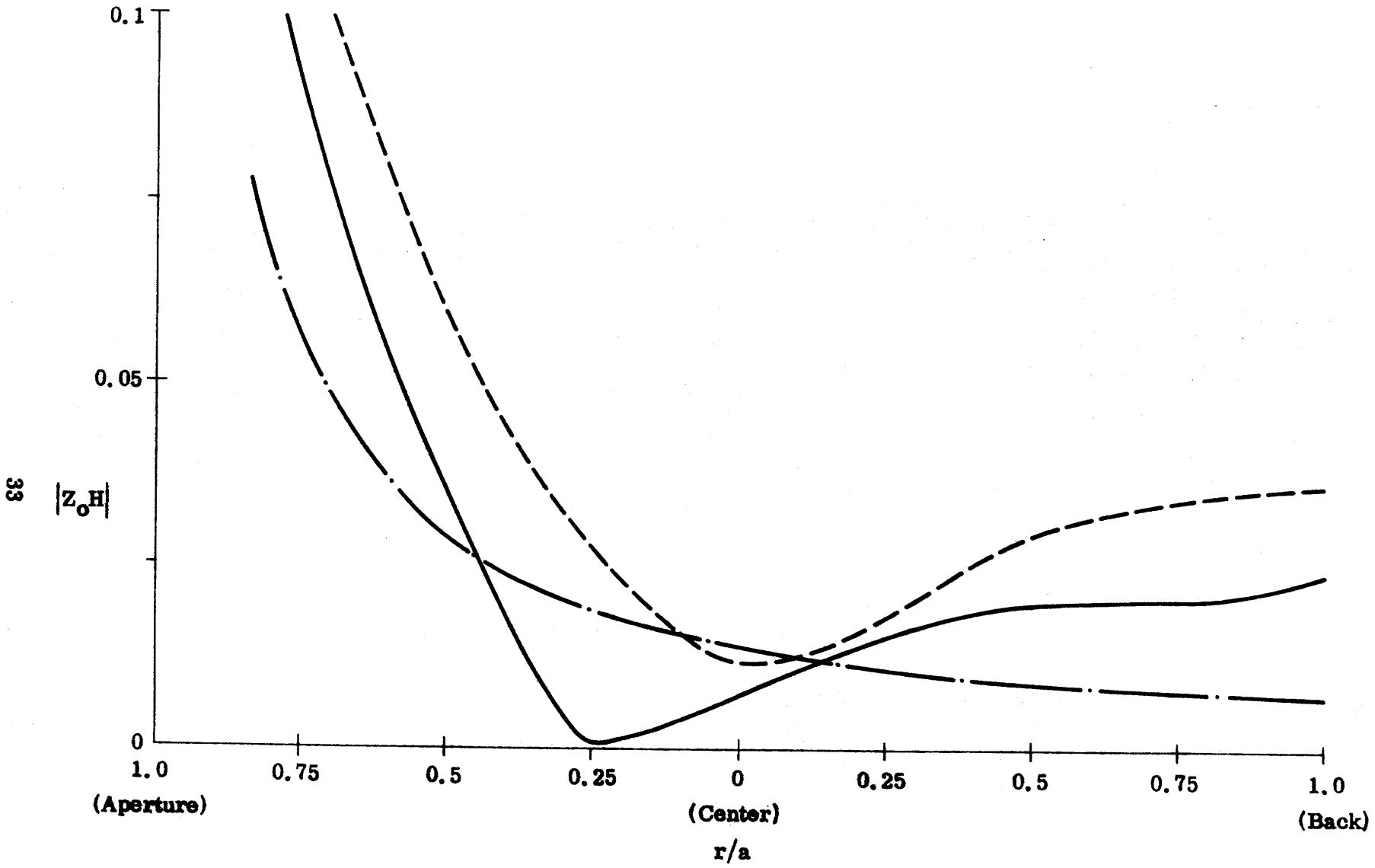


Fig. 18: Amplitude of the magnetic field along the main diameter of ka = 2.5, $\theta_o = 10^o$: exact (——), approx. A with $\gamma = 0.6$ (——), approx. D (— · —).

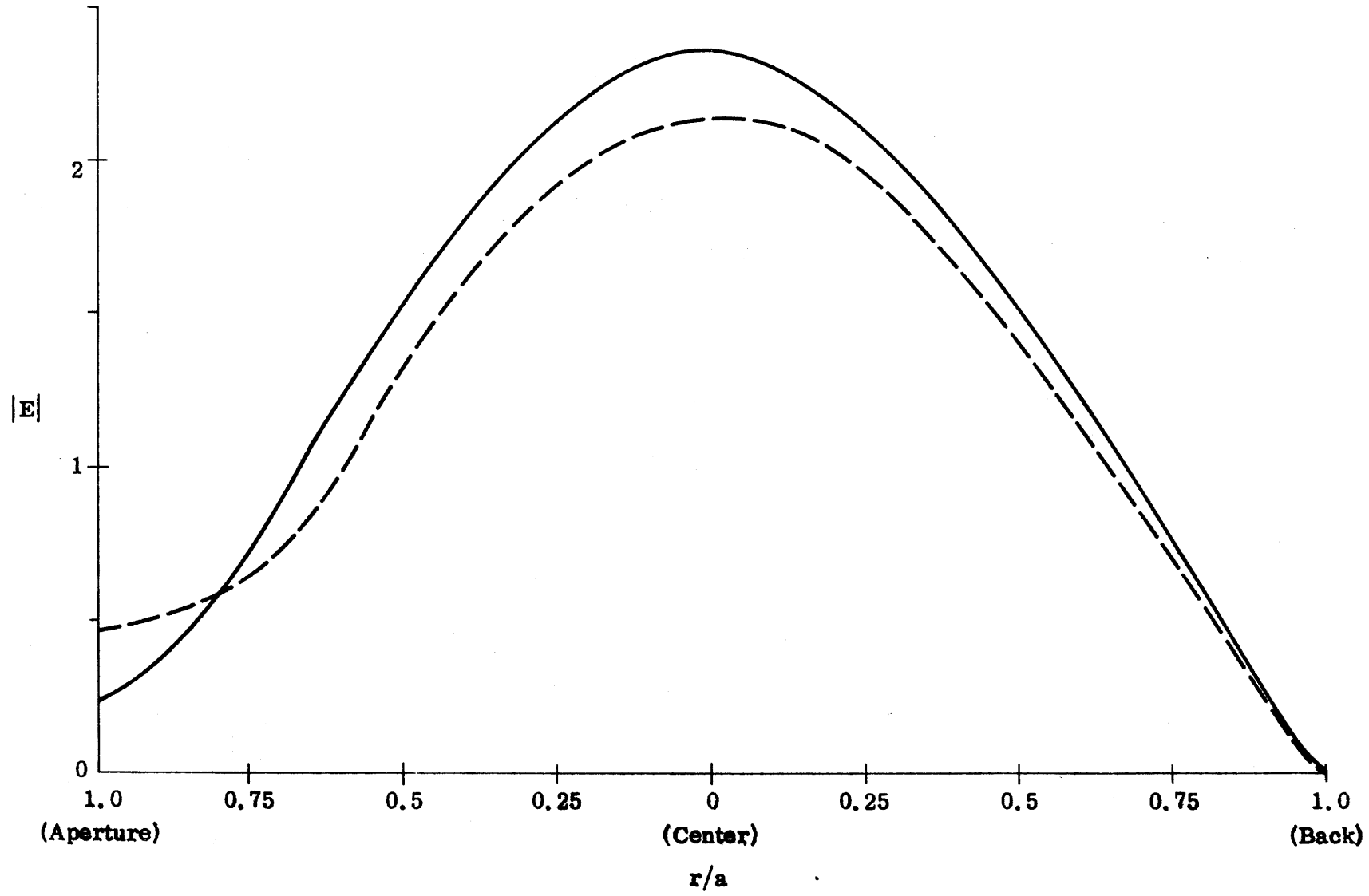


Fig. 19: Amplitude of the electric field along the main diameter for ka = 2.75, $\theta_o = 10^o$: exact (——), approx. A with $\gamma = 0.5$ (– – –).

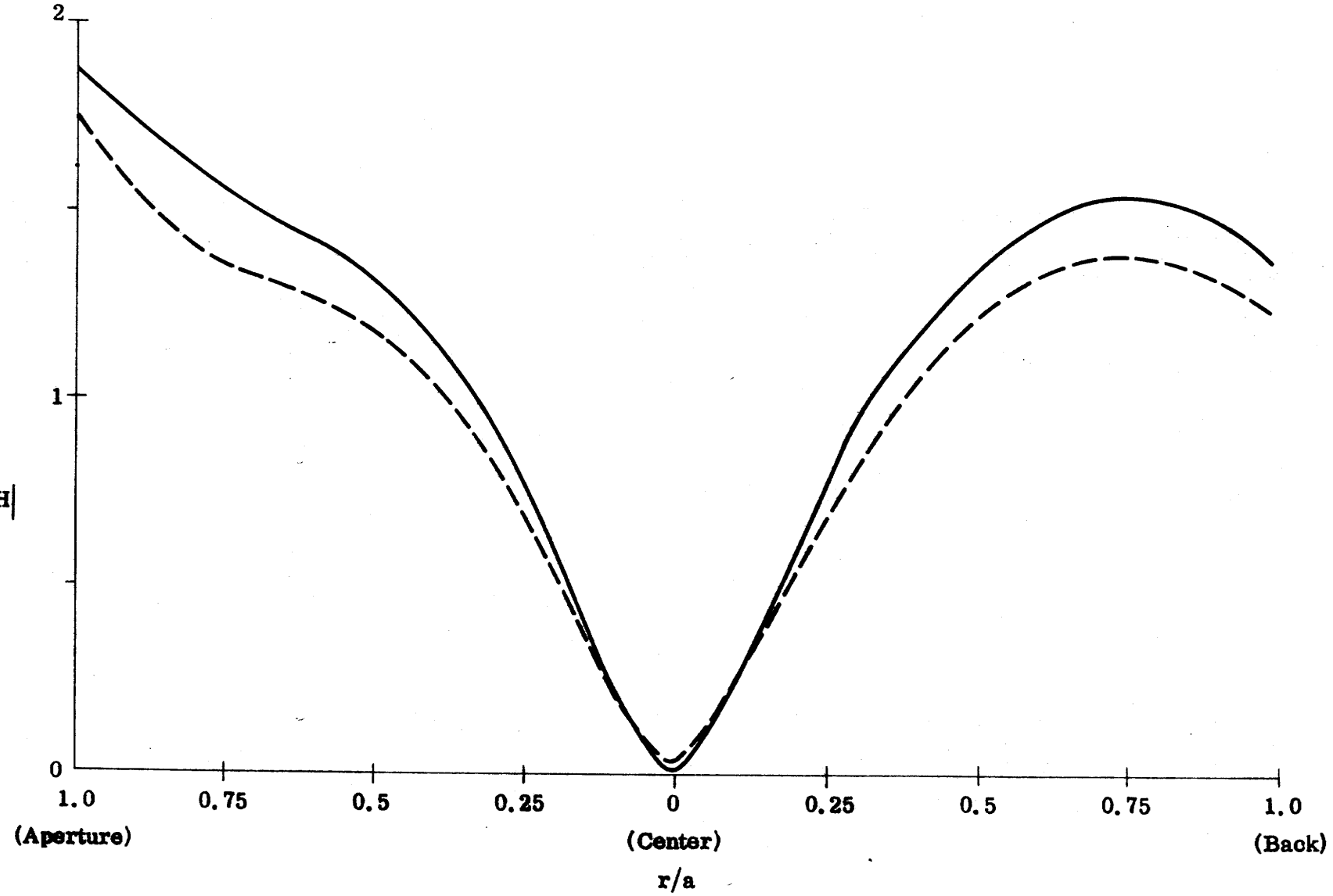


Fig. 20: Amplitude of the magnetic field along the main diameter for ka = 2.75, $\theta_o = 10^o$: exact (——), approx. A with $\gamma = 0.5$ (– – –).

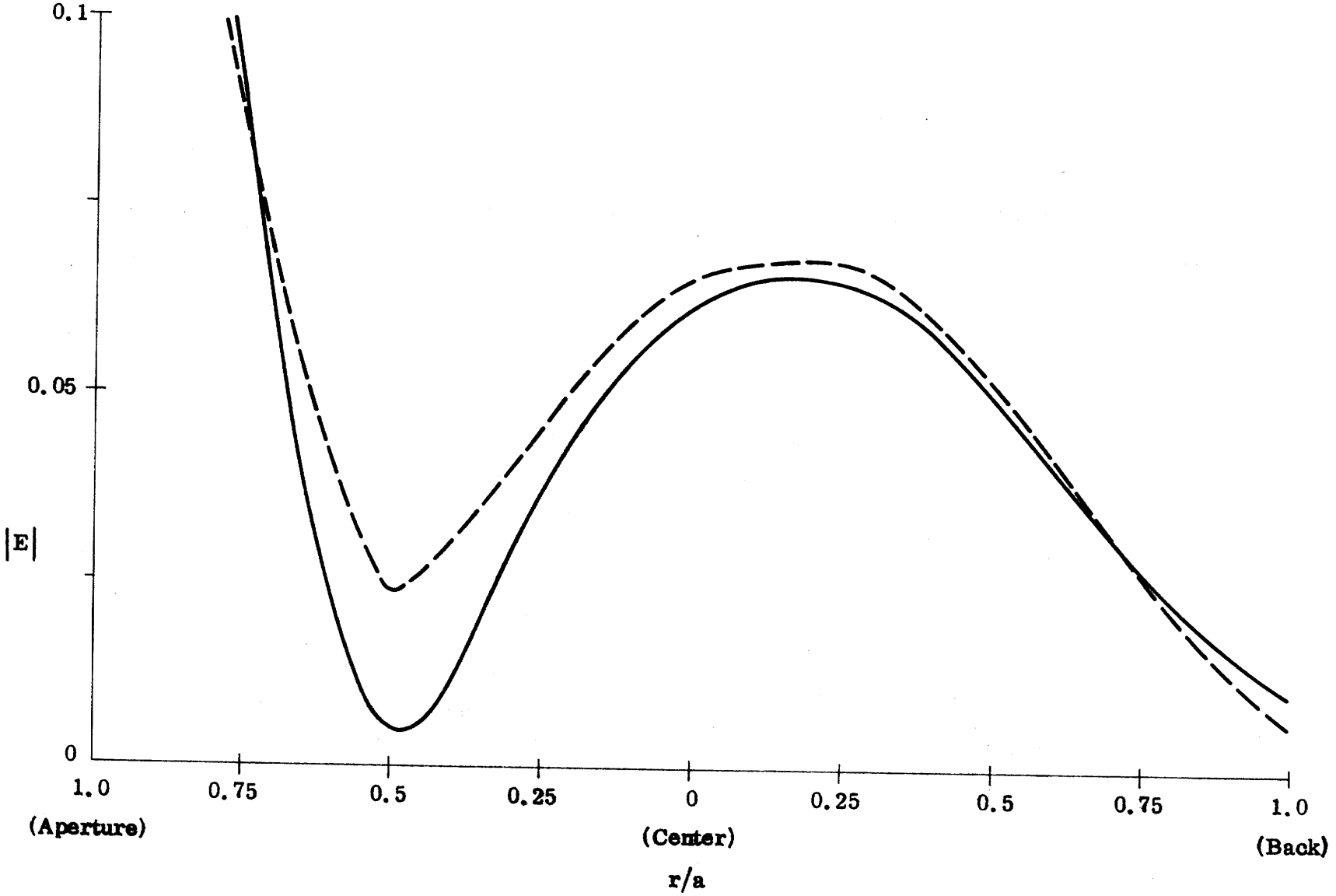


Fig. 21: Amplitude of the electric field along the main diameter for ka = 3.0, $\theta_o = 10^o$: exact (——), approx. A with $\gamma = 0.6$ (– – –).

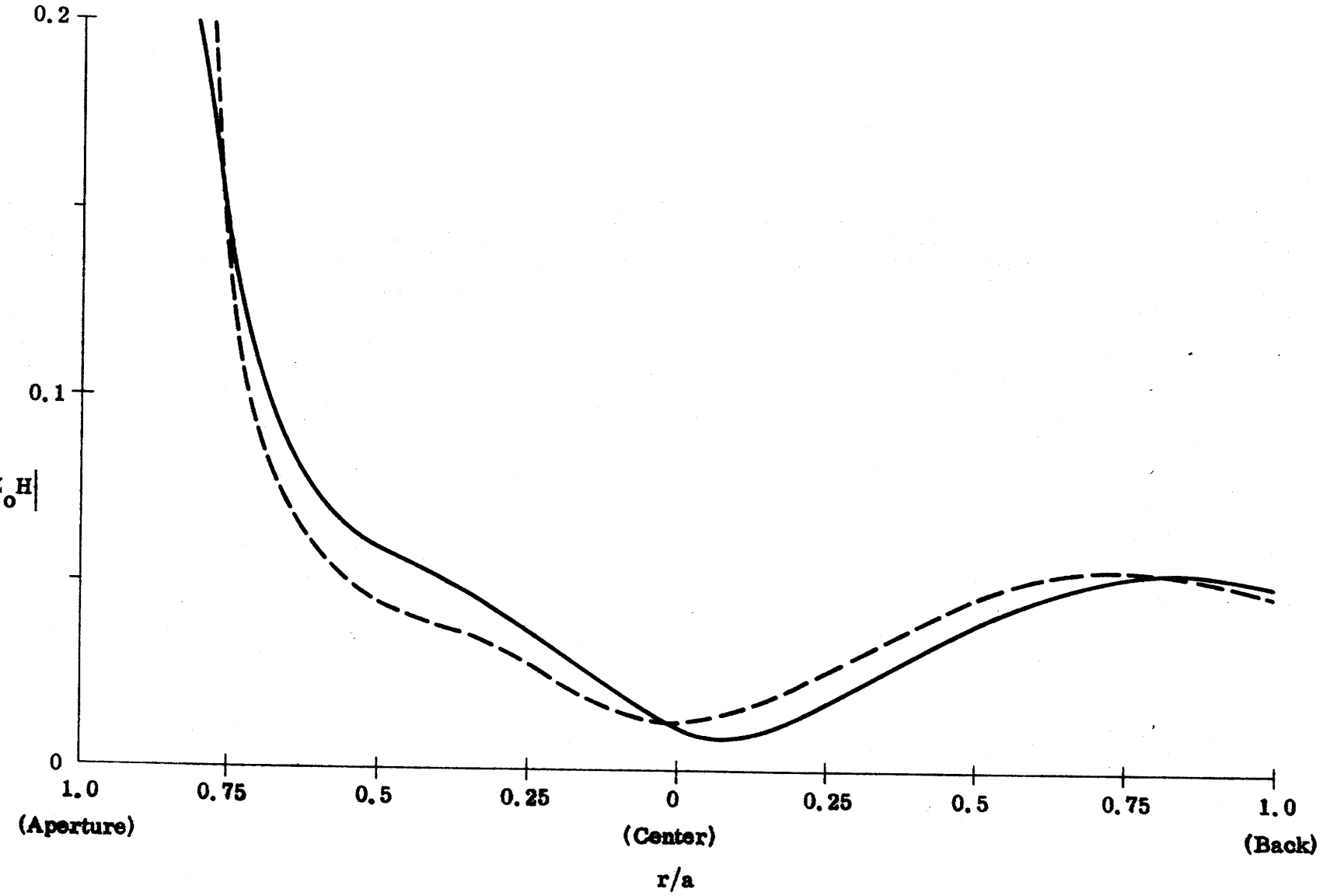


Fig. 22: Amplitude of the magnetic field along the main diameter for ka = 3.0, $\theta_o = 10^o$: exact (——), approx. A with $\gamma = 0.6$ (‹——).

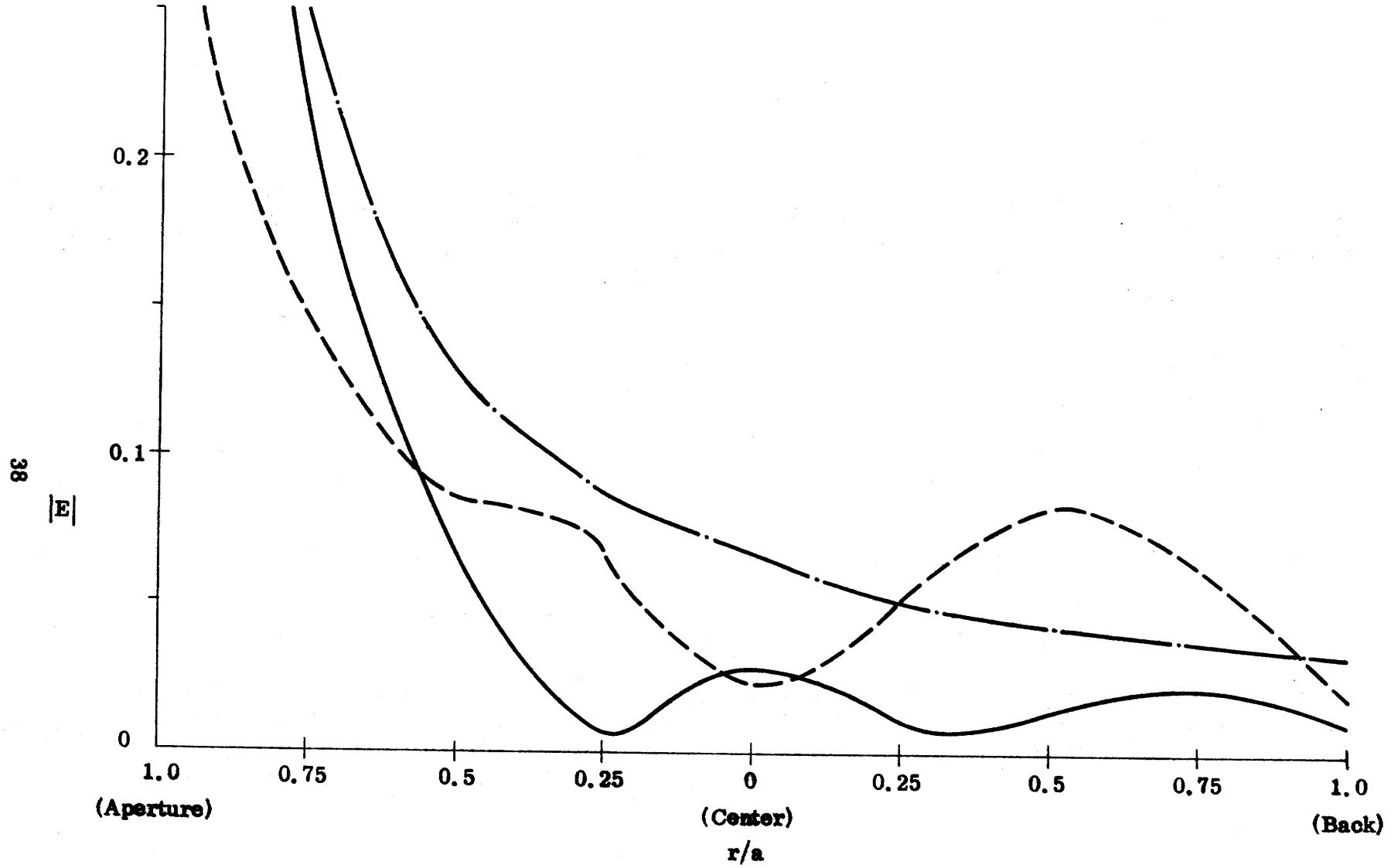


Fig. 23: Amplitude of the electric field along the main diameter for ka = 4.25, $\theta_o = 10^o$: exact (——), approx. A with $\gamma = 0.7$ (– – –), approx. C (— · —).

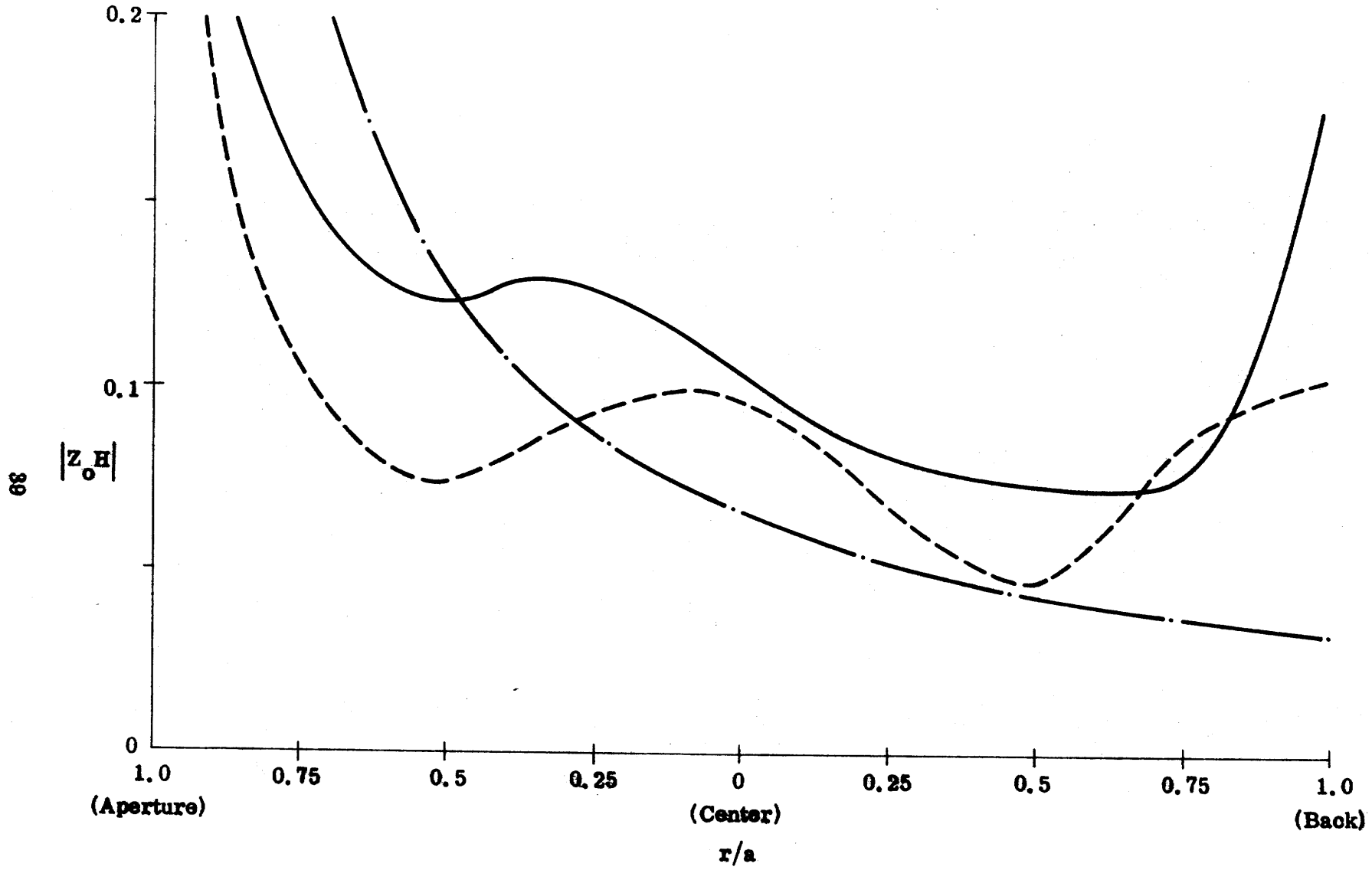


Fig. 24: Amplitude of the magnetic field along the main diameter for $ka = 4.25$, $\theta_o = 10^o$: exact (——), approx. A with $\gamma = 0.7$ (——), approx. C (— · —).

tion: ka = 1.0, 2.5, 2.75, 3.0 and 4.25. The data for ka = 1.0 are typical of low (below resonance) frequencies, and the results for ka = 4.25 illustrate the high frequency behavior of the fields. The intermediate values were selected to span the resonance at ka = 2.75. Data for both apertures are included, and though the results are given in the form of curves, it should be remembered that the computed values from which these were constructed were relatively sparse (9 values for each curve).

These same figures also show the field behaviors predicted using one or more of the approximate methods discussed in the previous Chapter. The first was based on the approximation (12) to the aperture distribution and a curve (labelled A) showing the resulting field behavior has been included in all of the Figs. 5 through 24. The scaling factors $\gamma$ were chosen visually to give a 'best fit' to the exact curves for the electric and magnetic fields. The factors that were used are listed on the Figures and again in Tables 1 and 2, which also contain

Table 1 ($\theta_o = 30^o$)

| ka | $\gamma$ | E at $\theta = 0$ (exact) |
|---|---|---|
| 1.0 | 0.7 | 0.63 |
| 2.5 | 2.5 | 2.5 |
| 2.75 | 0.1 | 0.293 |
| 3.0 | 1.8 | 1.8 |
| 3.5 | 3.0 | 2.55 |
| 4.25 | 2.6 | 2.6 |
| 5.0 | 0.26 | 0.63 |

the factors for some data that have not been included in this Note. The last column of the Tables shows the exact amplitude of the electric field at the center, $\theta = 0$, of the aperture.

Table 2 ($\theta_o = 10^o$)

| ka | $\gamma$ | E at $\theta = 0$ (exact) |
|---|---|---|
| 1.0 | 0.2 | 0.1 |
| 2.5 | 0.6 | 0.37 |
| 2.75 | 0.5 | 0.197 |
| 3.0 | 0.6 | 0.675 |
| 4.25 | 0.7 | 0.97 |

The last two approximations considered in Chapter 2 are cruder in that the presence of the cavity is neglected entirely. Nevertheless, the interior fields which they predict have been computed for some of the parameter combinations and the resulting curves included for purposes of comparison. The curves based on eq. (16) are labelled C and have been plotted in Figs. 13, 14, 23 and 24 for which the aperture is electrically large, whilst those based on (17) are labelled D and plotted in the small aperture cases (Figs. 5 through 8 and 15 through 18). Not surprisingly, these amplitudes are smooth, monotonically decreasing functions of a - z, and though they contain none of the structure which the exact fields display, they do predict the average values of the amplitudes to some degree.

Some idea of how the field intensities within the cavity vary as a function of frequency can be obtained from Fig. 25 in which the exact normalised energy density $|E|^2 + |Z_o H|^2$ at the center of the cavity is plotted as a function of ka for each of the two apertures. The resonances at ka = 2.75 and 4.49 are clearly seen, but are more pronounced for the smaller aperture: indeed, it would appear that the larger aperture has significantly de-tuned the cavity, and though Fig. 25 might suggest that the resonant values for $\theta_o = 10^o$ are no higher than the ones for $\theta_o = 30^o$, the sparseness of the data points does not enable us to determine the former precisely. At non-resonant frequencies, the

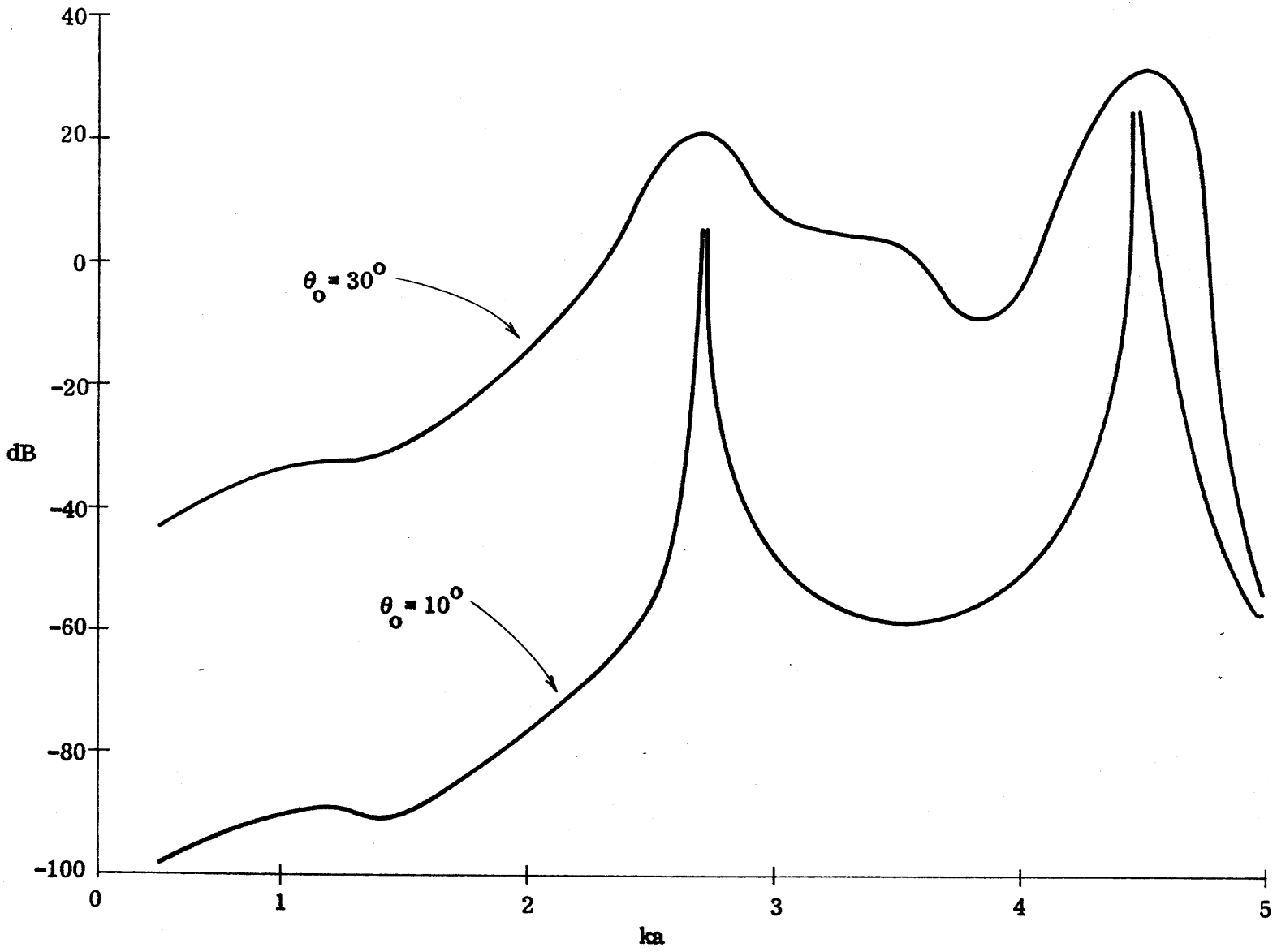


Fig. 25: Normalised energy density at r = 0.

density for $\theta_o = 30^o$ exceeds that for $\theta_o = 10^o$ by as much as 60 dB.

Our final comment is concerned with the computational time involved in the generation of the data. The Chang-Senior program is, of course, the most accurate of the ones discussed and is, in theory at least, capable of yielding data of any desired accuracy. But practice is another thing, and the necessity for truncating series which are rather slowly convergent is an obvious source of error. Even with these compromises, the program is still extremely expensive to run and for any given accuracy, the cost increases with ka. Thus, for $ka = 4.0$ and $\theta_o = 30^o$, the C. P. U. time needed to generate the data is between 50 and 60 seconds and the amount of core required is about 500,000 8-bit bytes. In contrast, the approximate methods discussed are much more efficient. To postulate the aperture distribution in the form (12) decreases the cost by a factor 20 and though this factor would be slightly reduced were we to implement a direct calculation of $\gamma$, it would still seem desirable to pursue this method further. If, finally, we neglect the cavity entirely and use either of the approximations C and D, the cost is less than one percent of that for the Chang-Senior program. However, the utility of the results obtained is not without question.

## 4. Discussion

A 'rigorous' analysis such as that provided by Chang and Senior (1969) is feasible only for the most idealised aperture-cavity configurations, and to determine the interior fields in more practical situations, it is essential to rely on approximate methods. In addition to the computation of the exact fields inside the spherical cavity, an objective of the present study was to examine some of the approximate methods that are available, and in this context the exact data becomes even more important in providing a basis with which to assess the accuracy of these approximations. Admittedly, a sphere with a circular hole is a very special geometry and there is no guarantee that a method which is accurate here will prove equally accurate in more general situations, but in the absence of an exact solution for any other geometry, these data are all that we have to go on.

The electromagnetic field behavior inside the cavity can be judged from the exact data in Figs. 5 through 24 showing the variation of the electric and magnetic field amplitudes along the main diameter. In general, the form of the curves is mainly determined by ka, with the aperture half angle $\theta_o$ affecting the amplitude. When ka is small, the fields show an almost exponential decrease away from the aperture. For $\theta_o = 10^o$, this same behavior obtains even for ka as large as 2.5, but with the larger aperture the influence of the first resonance is already detectable because of the detuning (see Fig. 25) which the aperture produces. This first resonance is at ka = 2.75 and the field distributions are now characteristic of the fundamental mode in a spherical cavity. When ka is increased to 3.0, we again see a rather rapid decrease in the field amplitudes immediately adjacent to the aperture, but over the remaining three-quarters of the main diameter, the behavior is oscillatory. As ka is increased still further (to 4.25), the patterns become more involved, and a simple description is no longer possible.

This complexity, however, does not seem to characterise the aperture fields. Plots of $|f|$ and $|g|$ for ka = 2.5 are given in Figs. 3 and 4 and apart from a scaling factor, these are typical of all the values of ka for which data has been obtained. In other words, for an aperture of fixed electrical size, the main influence that ka has is to produce a scaling in amplitude. Rather surprisingly, this seems true even at the resonant frequencies of the cavity. Within a distance of about $0.05\lambda$ from the edges, the aperture fields are dominated by edge effects, but over the remainder of the aperture, the amplitudes are relatively constant apart from a small superimposed high frequency oscillation. Since oscillatory fields of this type cannot radiate and are primarily associated with energy stored in the vicinity of the aperture, it is reasonable to expect that the main source of the cavity fields is the combination of the 'constant' and edge-dominated distributions. In contrast, the high frequency structure of the aperture field is important only at small distances, and has little effect on the fields throughout the rest of the cavity.

In view of the above findings it is not surprising that the first of the approximate methods discussed in Chapter 3 is quite effective in predicting the field distributions within the cavity. The curves based on the approximation (12) with the scaling factor $\gamma$ chosen to produce a 'best fit' to the exact data are included in all of Figs. 5 through 24. In general the agreement is quite good, even for the case ka = 1.0 and $\theta_o = 10^o$ (Figs. 15 and 16) where the aperture is only $0.055\lambda$ across; where there are major discrepancies, these tend to be confined to the portions of the cavity closest to the aperture. According to the approximation (12), the amplitude of the electric field at the center, $\theta = 0$, of the aperture is $\gamma$, and in Tables 1 and 2 the values of $\gamma$ used in Figs. 5 through 24 are compared with the exact values of $|E|$ at this point. For the larger aperture the agreement is remarkably good, with the only significant discrepancies occuring at ka = 2.75 (the lowest resonance) and ka = 5.0 (which is close to the magnetic mode resonance,

ka = 4.97, corresponding to the first zero of $\psi_3'(ka)$). The agreement is much poorer for $\theta_o = 10^o$, and this may be due to the proportionately larger part of the aperture over which the edge behavior dominates. If this is so, the agreement could be improved by combining the edge distribution (13) over the extreme portion of the aperture with the incident field form (12) over the remainder.

Table 3 lists the exact electric field amplitude at the center of the $30^o$

Table 3

| ka | E $\begin{matrix} r=a \\ \theta=0 \end{matrix}$ | ka | E $\begin{matrix} r=a \\ \theta=0 \end{matrix}$ |
|---|---|---|---|
| 0.5 | 0.33 | 2.75 | 0.29 |
| 0.75 | 0.38 | 3.0 | 1.81 |
| 1.00 | 0.63 | 3.25 | 2.45 |
| 1.25 | 0.85 | 3.5 | 2.55 |
| 1.5 | 0.99 | 3.75 | 1.03 |
| 1.75 | 1.24 | 4.0 | 1.52 |
| 2.00 | 1.18 | 4.25 | 2.6 |
| 2.25 | 1.7 | 4.5 | 0.189 |
| 2.5 | 2.5 | 4.75 | 2.21 |
| | | 5.0 | 0.634 |

half-angle aperture for all of the values of ka for which data has been computed. The amplitude increases rather uniformly with increasing ka, reaching a maximum of around 2.5 at ka $\simeq$ 2.5 and then drops to a very low level at the resonant frequency, ka = 2.75. Thereafter, the amplitude again increases to 2.5 before dropping at the next resonance, ka = 3.87, and so on. To judge from these data, the peak amplitudes do not exceed about 2.5. At non-resonant frequencies, the fields within the cavity initially decrease away from the aperture, and though they may later increase, the maximum energy density achieved is less than that

at the center of the aperture. At a resonant frequency, however, the reverse is true. The fields now increase away from the aperture and the maximum energy density occurs in the interior of the cavity. In combination with Table 3, these facts suggest that the field levels within the cavity can be bounded by using the approximation (12) in conjunction with the value $\gamma = 2.5$. This will significantly overestimate the fields at any resonant frequency of the cavity, and here a somewhat closer upper bound could be had by choosing (say) $\gamma = 1.0$.

With the last two approximations considered in Chapter 3, the presence of the cavity was ignored entirely. The corresponding formulae for the 'interior' fields are given in eqs. (16) and (17), and since, in both cases, the fields decrease with increasing distance from the aperture, it is at once obvious that the predictions will be inadequate near any resonant frequency. The curves based on the small aperture approximation (17) are labelled D and have been included in Figs 5 through 8 and 15 through 18 for $ka = 1.0$ and 2.5. Not surprisingly, the agreement with the exact curves gets poorer as the electrical size of the aperture increases, but even for $ka = 1.0$ and $\theta_o = 10^o$ the approximation is markedly inferior to that provided by the high frequency postulate (12)! Throughout most of the cavity the approximation underestimates the fields that are present and the discrepancy increases with increasing aperture size. Though it still has some merit for $ka = 2.5$ and $\theta_o = 10^o$, it fails completely at this frequency for the larger aperture due to its inability to display any resonance phenomena. The curves based on the large aperture approximation (16) have been computed only for $ka = 4.25$ and are labelled C in Figs. 13, 14, 23 and 24. Here also the agreement with the exact data is rather poor.

One purpose in pursuing these simpler approximations C and D was to use them to provide an estimate of the scaling factor $\gamma$ required in approximation A by (say) matching the fields predicted by A and C at the center of the cavity. The data we have obtained give no grounds for believing that this would be effective, and in spite of the greater time required for the computation of A, the superior

accuracy which this approximation affords appears more than adequate recompense. To realise this accuracy, however, it is necessary to compute the scaling factor $\gamma$ without recourse to a knowledge of the exact fields. A method was suggested in Chapter 2 and it would seem desirable to implement this in any future study. It would also be appropriate to consider a combination of the aperture fields (12) and (13) with (say) (13) being used over the extreme portions (of width $\sim 0.05\lambda$) of the aperture and (12) over the remainder. This would now be effective for apertures either large or small and, with $\gamma$ again determined by some form of matching across the aperture, should permit the calculation of the interior fields to a reasonable degree of accuracy.

References

Bailin, L. L., and S. Silver (1956), "Exterior electromagnetic boundary value problems for spheres and cones," IRE Trans. Ant. and Prop. AP-4, 5-16.

Bethe, H. A. (1944), "Theory of diffraction by small holes," Phys. Rev. 66, 163-182.

Chang, S., and T. B. A. Senior (1969), "Scattering by a spherical shell with a circular aperture," Univ. of Michigan Radiation Laboratory Report No. 1363-5-T, Interaction Note No. 141.

Enander, B. (1971), "Scattering by a spherical shell with a small circular aperture," Interaction Note No. 77.

Stratton, J. A. (1941), "Electromagnetic Theory," McGraw-Hill Book Co., Inc.

351 (49)